Article

Dissociable hindbrain GLP1R circuits for satiety and aversion

https://doi.org/10.1038/s41586-024-07685-6

Received: 18 March 2023

Accepted: 6 June 2024

Published online: 10 July 2024

Check for updates

Kuei-Pin Huang[1], Alisha A. Acosta[1], Misgana Y. Ghidewon[1,2,4], Aaron D. McKnight[1,2,4], Milena S. Almeida[1], Nathaniel T. Nyema[1], Nicholas D. Hanchak[1], Nisha Patel[1], Yenoukoume S. K. Gbenou[1], Alice E. Adriaenssens[3], Kevin A. Bolding[1,2] & Amber L. Alhadeff[1,2]✉

The most successful obesity therapeutics, glucagon-like peptide-1 receptor (GLP1R) agonists, cause aversive responses such as nausea and vomiting[1,2], effects that may contribute to their efficacy. Here, we investigated the brain circuits that link satiety to aversion, and unexpectedly discovered that the neural circuits mediating these effects are functionally separable. Systematic investigation across drug-accessible GLP1R populations revealed that only hindbrain neurons are required for the efficacy of GLP1-based obesity drugs. In vivo two-photon imaging of hindbrain GLP1R neurons demonstrated that most neurons are tuned to either nutritive or aversive stimuli, but not both. Furthermore, simultaneous imaging of hindbrain subregions indicated that area postrema (AP) GLP1R neurons are broadly responsive, whereas nucleus of the solitary tract (NTS) GLP1R neurons are biased towards nutritive stimuli. Strikingly, separate manipulation of these populations demonstrated that activation of NTS^{GLP1R} neurons triggers satiety in the absence of aversion, whereas activation of AP^{GLP1R} neurons triggers strong aversion with food intake reduction. Anatomical and behavioural analyses revealed that NTS^{GLP1R} and AP^{GLP1R} neurons send projections to different downstream brain regions to drive satiety and aversion, respectively. Importantly, GLP1R agonists reduce food intake even when the aversion pathway is inhibited. Overall, these findings highlight NTS^{GLP1R} neurons as a population that could be selectively targeted to promote weight loss while avoiding the adverse side effects that limit treatment adherence.

A long-standing question exists regarding the relationship between satiety and nausea. Although nausea can occur independently of physiological satiety, the feeling of nausea is nearly always accompanied by appetite loss. Despite its relevance to the lives of millions of people who experience nausea from drug treatment, disease, pregnancy or other conditions, whether nausea and satiety arise from similar or different neural circuits has remained unclear.

Addressing this question has become even more important as the effort to develop weight-loss therapeutics intensifies. With 2.6 billion people worldwide classified as overweight or obese[3], the lack of effective weight-loss strategies has become a pressing public health issue. One of the barriers to drug treatments for obesity is the incidence of aversive side effects, with nausea and vomiting at the top of this list[1,2]. These undesirable effects of weight-loss therapeutics limit treatment adherence and increase attrition, compromising treatment efficacy.

The most effective weight-loss drugs are the long-acting GLP1R agonists. Multiple generations of these therapies are clinically available, including exenatide (the synthetic exendin-4, known as Byetta), liraglutide (Saxenda) and the most effective and popular GLP1-based monotherapy, semaglutide (Ozempic and Wegovy), which results in an impressive reduction in body weight of around 16% in clinical trials[1,2]. GLP1R agonists are also critical components of newer dual- and tri-agonist strategies to treat obesity[4,5]. However, nausea is by far the most common adverse event for each of these pharmacotherapies, with up to 60% of participants reporting this side effect[1,2,4,5].

The development of a drug that inhibits food intake without inducing nausea would revolutionize our ability to treat obesity and associated diseases. However, this depends on the existence of dissociable GLP1R-mediated mechanisms for satiety and nausea/aversion. Here, we determine that the hindbrain is a major site of action for satiety and weight loss elicited by GLP1-based therapeutics, and discover that two functionally distinct projections arising from discrete populations of hindbrain GLP1R neurons mediate satiety and aversion. This mechanistic dissociation of the therapeutic and adverse effects of obesity drugs may enable the development of safer and more effective weight-loss drugs.

Obesity drugs act on hindbrain GLP1R neurons

Although there are GLP1R-expressing cells throughout the periphery (for example, in the pancreas, kidney, gastrointestinal tract and vagus nerve) and across the brain[6,7], peripherally delivered GLP1-based obesity

[1]Monell Chemical Senses Center, Philadelphia, PA, USA. [2]Department of Neuroscience, University of Pennsylvania, Philadelphia, PA, USA. [3]Department of Neuroscience, Physiology, and Pharmacology, University College London, London, UK. [4]These authors contributed equally: Misgana Y. Ghidewon, Aaron D. McKnight. ✉e-mail: aalhadeff@monell.org

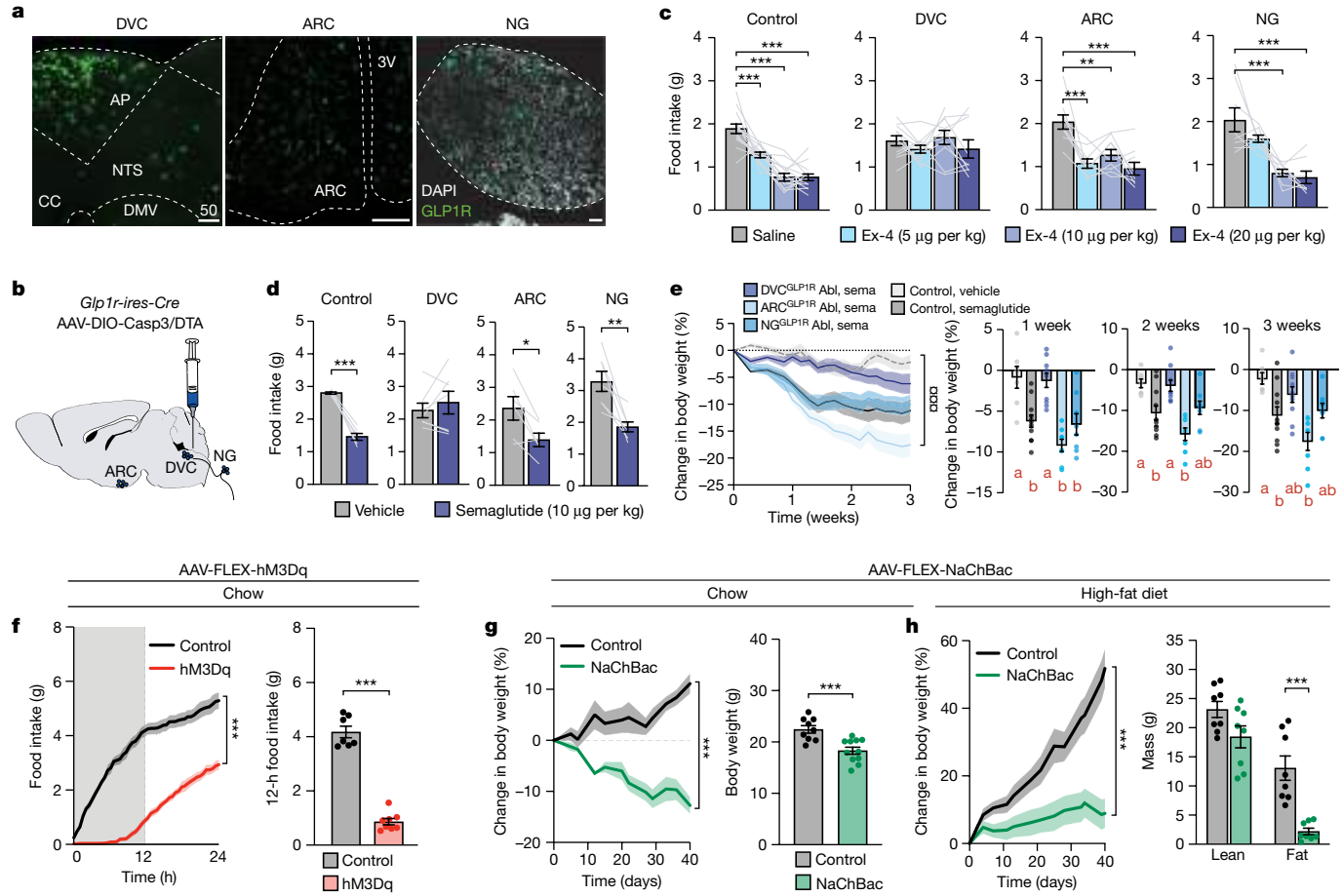

Fig. 1 | Hindbrain GLP1R neurons mediate the anorexic and weight-loss effects of GLP1-based obesity drugs. a, The mouse DVC, ARC and NG express GLP1R (in situ hybridization). 3V, third ventricle; CC, central canal, DMV, dorsal motor nucleus of the vagus nerve. Scale bars, 50 μm. **b**, Schematic for ablating GLP1R-expressing neurons in each region using an adenoassociated virus (AAV) encoding Cre-dependent Caspase3 (Casp3) or diphtheria toxin subunit A (DTA) in *Glp1r-ires-Cre* mice. **c**, Food intake after injection of saline or exendin-4 (Ex-4); $n = 8$–14 mice per group; one-way analysis of variance (ANOVA), $P < 0.01$ except for DVC, which was not significant (NS). **d**, Food intake after injection of vehicle or semaglutide; $n = 6$–7 mice per group; two-sided paired *t*-tests, $P < 0.05$ except for DVC which was NS. **e**, Left, percentage change in body weight; $n = 7$–11 mice per group, two-way repeated measures ANOVA, group × time interaction, $P < 0.001$. Right, percentage change in body weight at 1, 2 and 3 weeks; $n = 7$–11 mice per group; one-way ANOVA, red letters denote significantly different groups at $P < 0.05$. Abl, ablation; sema, semaglutide. **f**, Food intake over 24 h (left; $n = 7$–8 mice per group, two-way repeated measures ANOVA, control (chow) versus hM3Dq, $P < 0.001$; dark period indicated by grey shading) and in the dark period (right; $n = 7$–8 mice per group, two-sided unpaired *t*-test, control versus hM3Dq, $P < 0.001$). **g**, Change in body weight over time (left; $n = 9$–11 mice per group, two-way repeated measures ANOVA, control versus NaChBac, $P < 0.001$) and cumulative change in body weight (right; $n = 9$–11 mice per group, two-sided unpaired *t*-test, control versus NaChBac, $P < 0.001$). **h**, Change in body weight over time (left; $n = 9$–11 mice per group, two-way repeated measures ANOVA, control versus NaChBac, $P < 0.001$) and total lean and fat mass (right; $n = 8$ mice per group, two-sided unpaired *t*-test, control versus NaChBac, lean mass NS, fat mass $P < 0.001$). Values are mean ± s.e.m.; $^*P < 0.05$, $^{**}P < 0.01$, $^{***}P < 0.001$ for *t*-tests and post hoc comparisons; ¤¤¤$P < 0.001$ for two-way repeated measures ANOVA interaction. Letters denote significantly different groups at $P < 0.05$. See Supplementary Table 1 for statistical details for all figures and Extended Data figures.

drugs directly target neurons in the hindbrain dorsal vagal complex (DVC), the arcuate nucleus of the hypothalamus (ARC) and vagal afferents (the nodose ganglion, NG), and it is thought that action on GLP1R in these regions contributes to a reduction in food intake[8–10]. However, the necessity of each of these neural populations (Fig. 1a) in the anorexic and weight-loss effects of obesity therapeutics has not been systematically tested. To determine their contribution to GLP1R agonist-induced food intake suppression, we ablated each population by viral injections of Cre-dependent Caspase 3 (Casp3), diphtheria toxin subunit A (DTA) or a control virus (EGFP) in *Glp1r-ires-Cre* mice (Fig. 1b). These manipulations selectively ablated the DVC, ARC or NG GLP1R neurons without influencing the other GLP1R populations (Extended Data Fig. 1a–c). Ablation of DVC^{GLP1R} neurons, but not the populations in the ARC or NG, completely blocked food intake suppression by both exendin-4 (exenatide, the first GLP1-based drug approved by the US Food and Drug Administration; Fig. 1c and Extended Data Fig. 1d) and semaglutide (the most effective and most-recently approved GLP1-based obesity drug; Fig. 1d). Although there were no significant body-weight differences between the groups at baseline (Extended Data Fig. 1e), ablation of DVC^{GLP1R} neurons also blunted the long-term prevention of weight gain by semaglutide in mice maintained on a high-fat diet (Extended Data Fig. 1f–i). Most importantly, ablation of DVC^{GLP1R} neurons, but not ablation of ARC^{GLP1R} or NG^{GLP1R} neurons, blunted weight loss by semaglutide in obese mice (Fig. 1e), demonstrating the necessity of DVC^{GLP1R} neurons for the efficacy of this obesity drug. Together, these data highlight the DVC as a critical site of action for GLP1R-mediated weight-loss therapeutics.

We next tested how activation of DVC^{GLP1R} neurons influences feeding behaviour. Acute chemogenetic (hM3Dq) activation of DVC^{GLP1R} neurons potently suppressed food intake in food-deprived mice (Fig. 1f). To determine whether chronic activation of DVC^{GLP1R} neurons influences long-term energy balance, we injected *Glp1r-ires-Cre* mice in

the DVC with a Cre-dependent virus encoding NaChBac, a modified bacterial sodium channel that chronically upregulates neural activity. Chronic activation of DVC^{GLP1R} neurons not only reduced body weight in lean, chow-fed mice (Fig. 1g) but also prevented weight gain and fat mass accumulation in mice maintained on a high-fat diet (Fig. 1h). These effects were mediated by suppression of food intake through increased satiety, indicated by increased inter-meal interval and no change in meal size (Extended Data Fig. 2a–d), and not by changes in energy expenditure, because acute or chronic activation of DVC^{GLP1R} neurons decreased total energy expenditure (Extended Data Fig. 2e–h). Together, these data demonstrate the power of hindbrain GLP1R neuron activity in reducing food intake and preventing weight gain, and indicate that these neurons are a critical population of drug-accessible neurons responsible for the efficacy of GLP1-based obesity therapeutics.

In vivo activity in AP^{GLP1R} and NTS^{GLP1R} neurons

We next investigated how DVC^{GLP1R} neurons are engaged by obesity drugs and other anorexigenic stimuli. In the DVC, the AP and NTS both express GLP1R[11,12] (Fig. 2a,b and Extended Data Fig. 3a,b), and these regions are both implicated in food intake control and nausea-like behaviours[13–15]. We therefore sought to find differences in the neural activity patterns of AP^{GLP1R} and NTS^{GLP1R} neurons. We first created a 3D reconstruction of these populations after injecting *Glp1r-ires-Cre* mice with a Cre-dependent virus expressing a soma-restricted fluorophore and imaging cleared brain tissue. This approach enabled clear visualization of the two main populations of GLP1R neurons in the AP and the NTS, as well as a much smaller, caudal–lateral population in the cuneate nucleus (Fig. 2b and Supplementary Video 1), indicating that we can anatomically distinguish subregions of the DVC in intact tissue.

We therefore monitored in vivo neural activity in AP^{GLP1R} and NTS^{GLP1R} neurons in anaesthetized mice. We injected *Glp1r-ires-Cre*;*Ai9* mice with a virus expressing a Cre-dependent genetically encoded calcium indicator, GCaMP6s, and performed simultaneous two-photon imaging of the AP and NTS through a cranial window (Fig. 2c,d and Extended Data Fig. 3c–f). First, we monitored neural activity in response to semaglutide. Both AP^{GLP1R} and NTS^{GLP1R} neurons were significantly activated by semaglutide in comparison with vehicle administration (Fig. 2e–h), and similar proportions of neurons were activated in the AP and NTS (Extended Data Fig. 3g). Furthermore, the latency to semaglutide-induced activation was similar when comparing AP^{GLP1R} and NTS^{GLP1R} neurons (Extended Data Fig. 3h–j). Because GLP1R signalling causes both satiety and nausea/aversion[6,7], we next analysed responsivity to nutrients (Ensure, administered intraduodenally) or nauseogenic/aversive stimuli (cinacalcet or lithium chloride), both administered intravenously (Supplementary Video 2). Cinacalcet activates the calcium-sensing receptor (Casr), a G-protein-coupled receptor that is expressed in the AP and NTS[13,16,17] (Extended Data Fig. 8q) and causes nausea and aversion in humans and mice[13,18,19]. Overall, most activated DVC^{GLP1R} neurons were responsive to either Ensure or cinacalcet, with few neurons (6%) responsive to both stimuli (Fig. 2i). Moreover, most AP^{GLP1R} neurons were activated by the aversive stimulus (cinacalcet), whereas most NTS^{GLP1R} neurons were activated by the nutritive stimulus (Ensure) (Fig. 2i–p, Extended Data Fig. 4a–e and Extended Data Fig. 5). Visualization of a tuning index based on responsivity to Ensure and cinacalcet (see Methods for details) for each neuron similarly depicts differences in neural activity between AP^{GLP1R} and NTS^{GLP1R} neurons (Fig. 2l and Extended Data Fig. 4e). The products of the probabilities of a neuron being responsive to either Ensure or cinacalcet were significantly greater than the probability of a neuron being responsive to both stimuli in both the AP and the NTS (Extended Data Fig. 4g), indicating the existence of distinct functional subtypes of neurons in the AP and NTS. We next monitored neural activity in response to a different aversive stimulus, LiCl. When comparing calcium responses to nutrients with those to LiCl, there was also a bias in responsivity, but only in the NTS, which was again more tuned to Ensure than to the aversive stimulus, LiCl (Fig. 2m–p and Extended Data Fig. 4f). Overall, average neural activity responses to nutritive and aversive stimuli were generally consistent across mice, with greater responses to nutrients in NTS^{GLP1R} neurons and greater responses to aversive stimuli in AP^{GLP1R} neurons (Fig. 2j,k,n,o). Interestingly, across AP^{GLP1R} and NTS^{GLP1R} neurons, there were subpopulations of nutrient-responsive and aversion-responsive neurons that were inhibited by the other stimulus (Extended Data Fig. 4d,f). By contrast, very few neurons were inhibited by control solutions (Fig. 2e,f and Extended Data Fig. 4a) or by semaglutide (Fig. 2e,f). Overall, these findings indicate that DVC^{GLP1R} neurons are broadly activated by GLP1-based obesity drugs, but that individual neurons are tuned to nutritive or aversive stimuli. Furthermore, there are differences in subregion responses to nutritive and aversive stimuli, with NTS^{GLP1R} neurons being biased towards responsivity to nutritive rather than to aversive or nauseogenic stimuli.

Dissociable effects of AP^{GLP1R} and NTS^{GLP1R} neurons

GLP1 drug-induced nausea and anorexia co-occur[20], but it is unknown whether these features are intrinsically linked as a mechanism for food intake suppression and weight loss. Given the differences in the responses of AP^{GLP1R} and NTS^{GLP1R} neurons to nutritive and aversive stimuli, we next tested whether neural activity in these populations contributes differentially to aversion. To accurately examine aversion responses, we designed an approach to measure hedonic and aversive orofacial taste reactivity[21,22] while activating GLP1R neurons (Fig. 3a). As a positive control, mice were implanted with intraoral cannulae and infused with quinine or solutions paired with cinacalcet or LiCl to characterize behavioural responses (Extended Data Fig. 6a,b and Supplementary Video 3). As expected from studies in rats[22], quinine-infused mice displayed fewer hedonic responses (rhythmic mouth movements, lateral tongue protrusions and paw licks) and more aversive responses (gaping, chin rubs and facilitated fluid rejection) (Extended Data Fig. 6c–f). Similarly, pairing cinacalcet or LiCl to a new hedonic flavour stimulus caused both real-time and conditioned aversive taste reactivity (Extended Data Fig. 6g–n).

To determine whether the activation of DVC^{GLP1R} neurons triggers aversion, we injected *Glp1r-ires-Cre* mice in the DVC with Cre-dependent hM3Dq and paired chemogenetic activation of DVC^{GLP1R} neurons with intraoral delivery of a novel flavour (Fig. 3a). After pairing, mice displayed fewer conditioned hedonic responses and more conditioned aversive responses than did control mice (Fig. 3b and Extended Data Fig. 6o–s). We complemented this result with data from the more commonly used conditioned flavour avoidance (CFA) assay (Fig. 3c). As expected[13], activation of DVC^{GLP1R} neurons conditioned flavour avoidance (Fig. 3d). We quantified the number of cells expressing hM3Dq in the DVC and found a negative correlation between the number of hM3Dq+ neurons in the AP, but not in the NTS, and CS+ intake (a measure of conditioned avoidance; Extended Data Fig. 7). This finding supports our in vivo calcium imaging data, which together indicate that AP^{GLP1R} neurons may drive anorexia by inducing nausea/aversion[13] and NTS^{GLP1R} neurons may drive food intake inhibition by aversion-independent mechanisms.

To directly test this hypothesis, we injected 20 nl of an adenoassociated virus (AAV2.2, which has limited diffusion compared with other serotypes[23]) encoding Cre-dependent hM3Dq to either region. This strategy enabled expression in AP or NTS neurons without spread into neighbouring regions (Fig. 3e and Extended Data Fig. 8a–d). Activation of either AP^{GLP1R} (Fig. 3f) or NTS^{GLP1R} (Fig. 3g) neurons inhibited food intake by the same magnitude (Fig. 3h). Furthermore, the magnitude of food intake inhibition by either AP^{GLP1R} or NTS^{GLP1R} neurons was

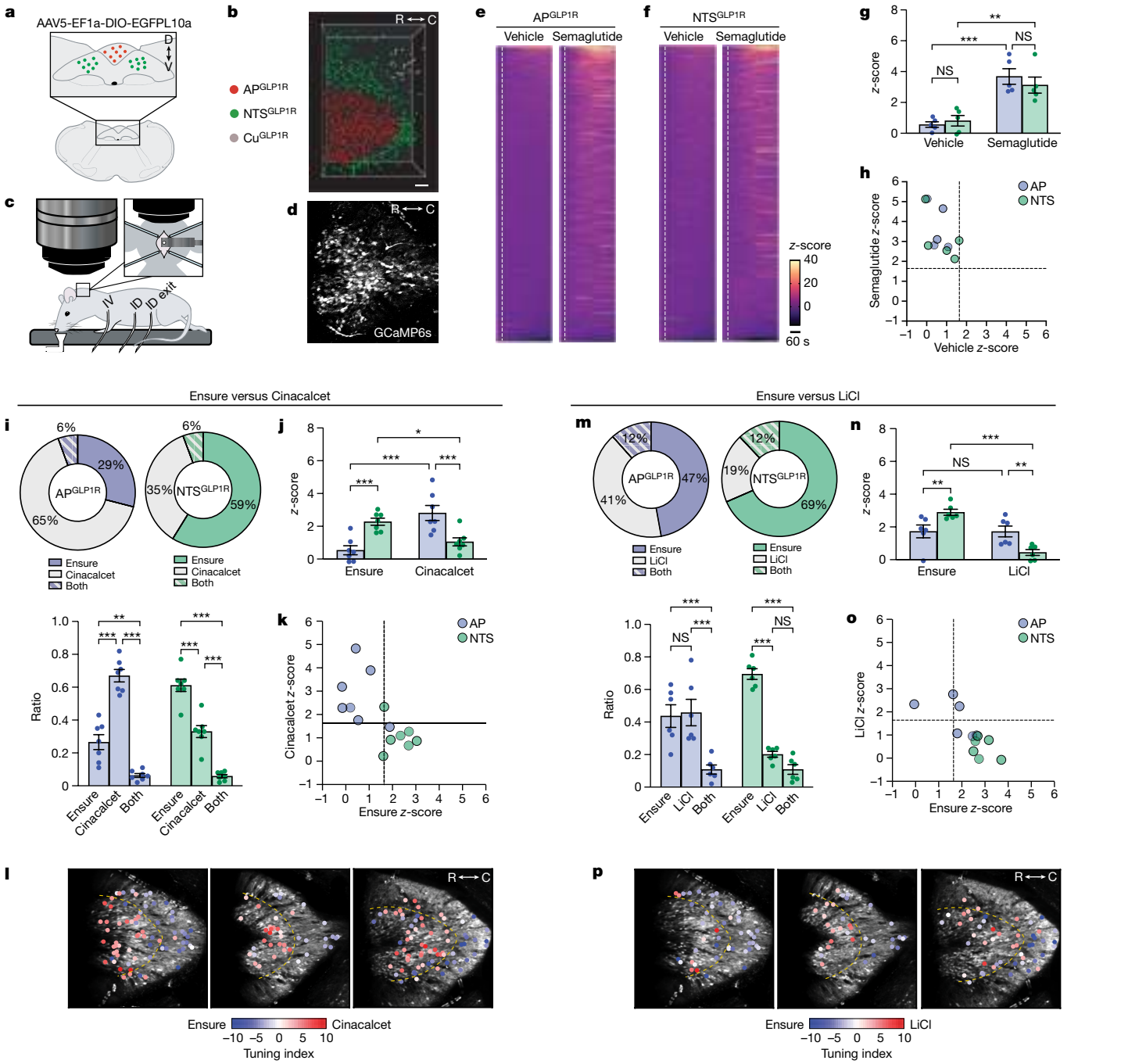

Fig. 2 | In vivo activity dynamics of AP^{GLP1R} and NTS^{GLP1R} neurons. a, Schematic of AP (red) and NTS (green) subregions of the DVC. **b**, Reconstruction of DVC^{GLP1R} populations in the AP, NTS and cuneate nucleus (Cu) after injection of a virus expressing a soma-restricted fluorophore. R, rostral; C, caudal. Scale bar, 100 µm. **c**, Schematic for simultaneous in vivo two-photon imaging of AP^{GLP1R} and NTS^{GLP1R} neurons. IV, intravenous; ID, intraduodenal. **d**, Representative two-photon maximum projection image of GCaMP6s expression in DVC^{GLP1R} neurons. **e**, The *z*-scored calcium responses of AP^{GLP1R} neurons to vehicle or semaglutide ($n = 787$ neurons, 5 mice). Dashed lines indicate the start of the stimulus. **f**, The *z*-scored responses of NTS^{GLP1R} neurons to vehicle or semaglutide ($n = 614$ neurons, 5 mice). **g**, Average *z*-scored responses of AP^{GLP1R} neurons (blue) and NTS^{GLP1R} neurons (green) to vehicle or semaglutide ($n = 5$ mice;, two-way ANOVA; AP, vehicle versus semaglutide, $P < 0.001$; NTS, vehicle versus semaglutide, $P < 0.01$). **h**, Comparison of AP^{GLP1R} and NTS^{GLP1R} neuron *z*-scored activity responses to vehicle and semaglutide. Dashed lines represent threshold for statistically significant activation. **i**, Proportions of activated AP^{GLP1R} neurons (left) and NTS^{GLP1R} neurons (right) responsive to Ensure, cinacalcet or both ($n = 7$ mice, two-way ANOVA, $P < 0.01$). **j**, Average *z*-scored responses in AP^{GLP1R} neurons (blue) and NTS^{GLP1R} neurons (green) to Ensure or cinacalcet ($n = 7$ mice, two-way ANOVA, $P < 0.05$). **k**, Comparison of AP^{GLP1R} and NTS^{GLP1R} neuron *z*-scored activity responses to Ensure and cinacalcet. **l**, Representative two-photon images of GCaMP6s with neurons colour-coded based on responses to Ensure (most responsive in blue, index = −10) and cinacalcet (most responsive in red, index = 10). The AP–NTS boundary is indicated by a yellow dashed line. **m**, Proportion of activated AP^{GLP1R} neurons (left) and NTS^{GLP1R} neurons (right) responsive to Ensure, LiCl or both ($n = 6$ mice, two-way ANOVA, $P < 0.001$ except AP, Ensure versus LiCl, NS, and NTS, LiCl versus both, NS). **n**, Average *z*-scored responses in AP^{GLP1R} neurons (blue) and NTS^{GLP1R} neurons (green) to Ensure or LiCl ($n = 6$ mice, two-way ANOVA, $P < 0.01$, except Ensure AP versus NTS, NS). **o**, Comparison of AP^{GLP1R} and NTS^{GLP1R} neuron *z*-scored activity responses to Ensure and LiCl. **p**, Representative two-photon images of GCaMP6s with neurons colour-coded based on responses to Ensure (most responsive in blue, index = −10) and cinacalcet (most responsive in red, index = 10). The AP–NTS boundary is indicated by a yellow dashed line. Values are mean ± s.e.m. $^*P < 0.05$, $^{**}P < 0.01$, $^{***}P < 0.001$.

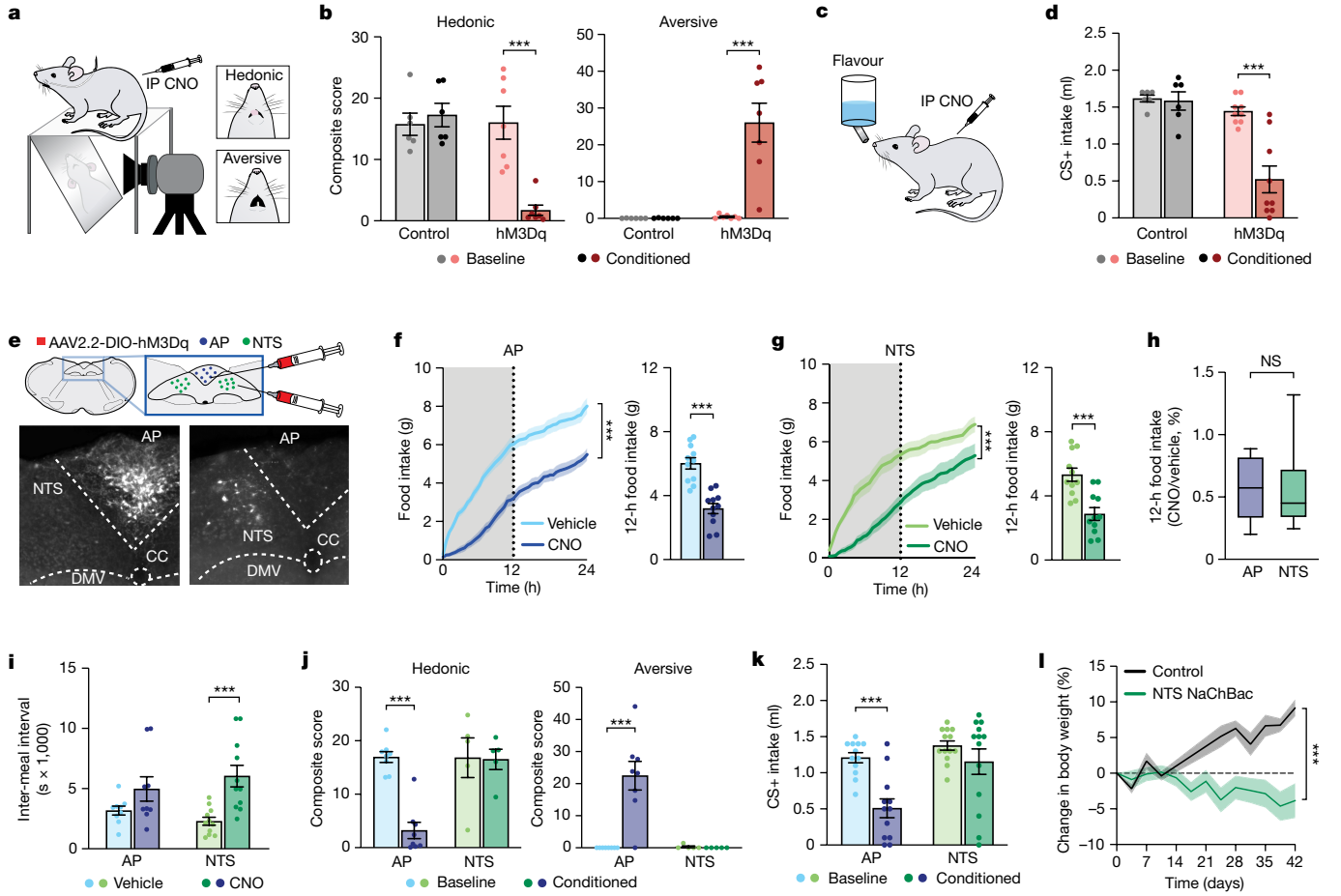

Fig. 3 | AP^{GLP1R} and NTS^{GLP1R} neurons drive aversion and satiety, respectively. **a**, Schematic of orofacial taste reactivity assay in *Glp1r-ires-Cre* mice showing example hedonic and aversive responses after intraperitoneal (IP) injection of clozapine *N*-oxide (CNO). **b**, Hedonic (left; $n = 6–7$ mice per group, two-way ANOVA, control baseline versus conditioned, NS; hM3Dq baseline versus conditioned, $P < 0.001$) and aversive (right; $n = 6–7$ mice per group, two-way ANOVA, control baseline versus conditioned, NS; hM3Dq baseline versus conditioned, $P < 0.001$) taste reactivity responses. **c**, Schematic of CFA assay. **d**, Intake of a flavour (CS+) paired with DVC^{GLP1R} neuron stimulation ($n = 6–9$ mice per group, two-way ANOVA, control baseline versus conditioned, NS; hM3Dq baseline versus conditioned, $P < 0.01$). **e**, Schematic (top) and representative images (bottom) of AAV2.2-hM3Dq in AP or NTS. **f**, Food intake over 24 h (left; $n = 11$ mice per group, two-way repeated measures ANOVA, vehicle versus CNO, $P < 0.001$) and in the dark period (right; $n = 11$ mice per group, two-sided unpaired *t*-test, vehicle versus CNO, $P < 0.001$) with chemogenetic (hM3Dq) activation of AP^{GLP1R} neurons. **g**, Food intake over 24 h (left; n = 11 mice per group, two-way repeated measures ANOVA, vehicle versus CNO, $P < 0.001$) and in the dark period (right; $n = 11$ mice per group, unpaired *t*-test, vehicle versus CNO, $P < 0.001$) with hM3Dq activation of NTS^{GLP1R} neurons. **h**, Food intake with AP^{GLP1R} or NTS^{GLP1R} neuron activation ($n = 11$ mice per group, two-sided unpaired *t*-test, AP^{GLP1R} versus NTS^{GLP1R} stimulation, NS). Box indicates median and first and third quartiles, bounded by minimum and maximum (whiskers). **i**, Inter-meal interval with AP^{GLP1R} or NTS^{GLP1R} neuron activation ($n = 9–11$ mice per group, two-way ANOVA, AP^{GLP1R} vehicle versus CNO, NS;, NTS^{GLP1R} vehicle versus CNO, $P < 0.01$). **j**, Hedonic (left; $n = 5–8$ mice per group, two-way ANOVA, AP^{GLP1R} baseline versus conditioned, $P < 0.001$; NTS^{GLP1R} baseline versus conditioned, NS) and aversive (right; $n = 5–8$ mice per group, two-way ANOVA, AP^{GLP1R} baseline versus conditioned, $P < 0.001$; NTS^{GLP1R} baseline versus conditioned, NS) taste reactivity responses. **k**, Intake of a flavour (CS+) paired with AP^{GLP1R} or NTS^{GLP1R} neuron stimulation ($n = 12–13$ mice per group, two-way ANOVA, AP^{GLP1R} baseline versus conditioned, $P < 0.001$; NTS^{GLP1R} baseline versus conditioned, NS). **l**, Change in body weight with chronic (NaChBac) or control (EGFP) NTS^{GLP1R} neuron activation ($n = 4$ mice per group, two-way repeated measures ANOVA, control versus NaChBac, $P < 0.001$). Values are mean ± s.e.m. $^*P < 0.05$, $^{**}P < 0.01$, $^{***}P < 0.001$.

comparable with the effect of DVC^{GLP1R} stimulation (that is, activating both AP^{GLP1R} or NTS^{GLP1R} neurons; Extended Data Fig. 8e,f). Activation of NTS^{GLP1R} neurons increased inter-meal interval (Fig. 3i) but had no effect on meal size (Extended Data Fig. 8g), indicating that NTS^{GLP1R} neurons increase satiety. There were no differences between the effects of AP^{GLP1R} or NTS^{GLP1R} neuron activation on energy expenditure (Extended Data Fig. 8h–j).

We next analysed the effects of AP^{GLP1R} and NTS^{GLP1R} neuron activity on aversion. Strikingly, activation of AP^{GLP1R} neurons, but not NTS^{GLP1R} neurons, reduced hedonic and increased aversive taste reactivity responses (Fig. 3j and Extended Data Fig. 8k–o). Similarly, activation of AP^{GLP1R} neurons[13], but not NTS^{GLP1R} neurons, was sufficient to condition a CFA (Fig. 3k). Importantly, chronic activation of NTS^{GLP1R} neurons was sufficient to reduce body weight (Fig. 3l). These data highlight NTS^{GLP1R} neurons as a population that inhibits food intake and reduces body weight without inducing aversion.

Finally, we combined and re-analysed three existing single cell and nucleus RNA sequencing datasets[13,16,17] to determine that AP^{GLP1R} and NTS^{GLP1R} neurons are mixed excitatory and inhibitory populations, with a greater proportion of NTS^{GLP1R} neurons being excitatory (Extended Data Fig. 8p,q). This analysis also indicated that AP^{GLP1R} and NTS^{GLP1R} neurons are largely distinct from other DVC cell types, such as CCK, Adacyap1, Tac1, Gcg and Calcr (Extended Data Fig. 8q). Together with our physiological and behavioural results, these data demonstrate that AP^{GLP1R} and NTS^{GLP1R} neurons are generally distinct from other hindbrain cell types and mediate aversion and satiety responses, respectively.

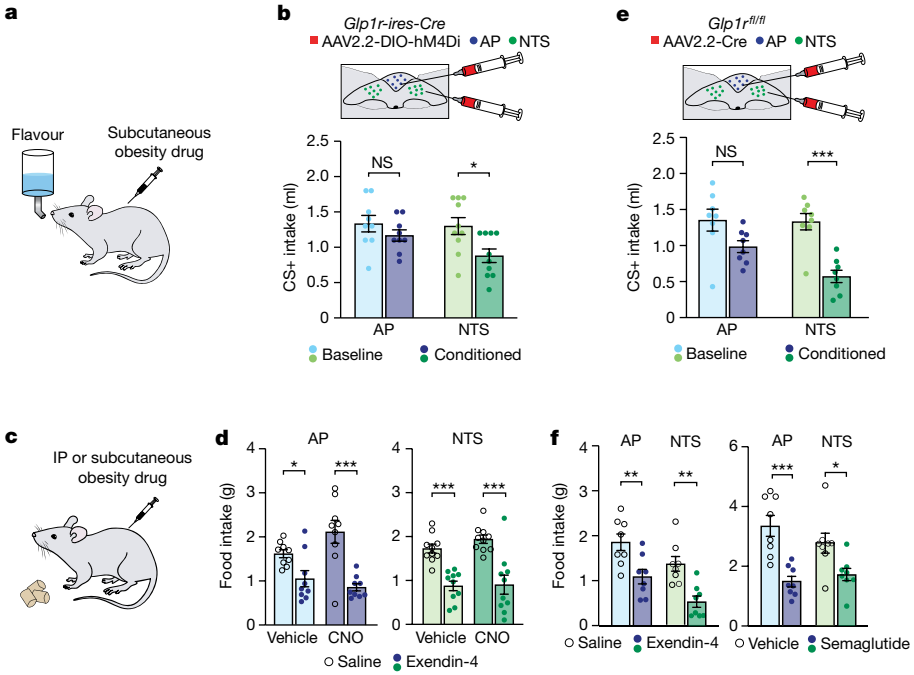

Fig. 4 | Obesity drugs reduce food intake when aversion circuitry (AP^{GLP1R} neurons) is blunted. a, Schematic of CFA assay. **b**, Intake of flavour (CS+) paired with semaglutide injection in mice with chemogenetic inhibition of AP^{GLP1R} or NTS^{GLP1R} neurons (n = 9–10 mice per group, two-way ANOVA, AP^{GLP1R} baseline versus conditioned, NS; NTS^{GLP1R} baseline versus conditioned, $P < 0.05$). **c**, Schematic for measuring food intake after injection of obesity drugs. For exendin-4 studies, food was returned immediately after injection. For semaglutide studies, food was returned 4 h after injection. **d**, Food intake in response to exendin-4 injection in mice with AP^{GLP1R} or NTS^{GLP1R} neuron inhibition (n = 9–10 mice per group, two-way ANOVA, $P < 0.05$). **e**, Intake of flavour (CS+) paired with semaglutide injection in mice with deletion of GLP1R in AP or NTS (n = 8 mice per group, two-way ANOVA, AP^{GLP1R} baseline versus conditioned, NS; NTS^{GLP1R} baseline versus conditioned, $P < 0.001$). **f**, Food intake in response to exendin-4 (left) or semaglutide (right) injection in mice with AP or NTS GLP1R deletion (n = 8 mice per group, two-way ANOVA, $P < 0.01$). Values are mean ± s.e.m. *$P < 0.05$, **$P < 0.01$, ***$P < 0.001$.

Aversion is not required for obesity drug effects

To determine whether obesity drugs are still effective at suppressing food intake when the aversion pathway is inhibited, we treated mice with GLP1-based obesity drugs and inhibited neural activity in AP^{GLP1R} or NTS^{GLP1R} neurons while measuring food intake and flavour avoidance. Chemogenetic inhibition (hM4Di) of AP^{GLP1R} neurons, but not of NTS^{GLP1R} neurons, blunted the CFA to a semaglutide-paired flavour (Fig. 4a,b). Importantly, however, inhibiting neural activity in either population did not block the food intake suppression by GLP1-based obesity drugs (Fig. 4c,d).

We next tested whether expression of GLP1R in AP or NTS neurons is necessary for the effects of GLP1-based obesity drugs on food intake and aversion. To achieve this, we deleted GLP1R from the DVC, AP or NTS by injecting *Glp1r$^{fl/fl}$* mice[24] with an AAV encoding Cre (Extended Data Fig. 9a,b). DVC^{GLP1R} deletion attenuated both the anorexic and aversive effects of semaglutide (Extended Data Fig. 9c–g). Similar to our chemogenetic inhibition results, deleting GLP1R from the AP, but not from the NTS, blunted the aversion responses to semaglutide (Fig. 4e). The deletion of AP^{GLP1R} or NTS^{GLP1R} did not affect anorexia induced by exendin-4 or semaglutide (Fig. 4f). These data demonstrate that the anorexic effect of GLP1-based obesity drugs remains intact even when the aversion pathway is inhibited, indicating that future drugs could be better targeted to promote satiety without aversion.

Projections of AP^{GLP1R} and NTS^{GLP1R} neurons

Our data demonstrate that AP^{GLP1R} and NTS^{GLP1R} neurons drive aversion and satiety, respectively. To determine the circuitry through which this occurs, we first performed whole-brain histological analysis after fluorophore (EYFP) labelling (Fig. 5a and Extended Data Fig. 10a–f) or H129-ΔTK-TT (tdTomato) anterograde tracing (Fig. 5b and Extended Data Fig. 10g) of DVC^{GLP1R} neurons. These data revealed ascending projections to two regions, the lateral parabrachial nucleus (lPBN) and the paraventricular hypothalamus (PVH), in a remarkably distinct projection pattern compared with the more-widespread projections of some other DVC subpopulations, such as TH[25], Gcg/GLP1[26] and POMC[27].

To test whether AP^{GLP1R} and NTS^{GLP1R} neurons have similar or divergent projections, we next injected pseudorabies virus (PRV-263) into either the lPBN or the PVH (Fig. 5c). This virus is taken up by axons and retrogradely transported by all cells to express tdTomato, and by Cre-expressing cells to express EYFP or mCerulean. Analysis of DVC sections indicated that AP^{GLP1R} and NTS^{GLP1R} neurons send largely separate projections to the lPBN and the PVH, respectively (Fig. 5c and Extended Data Fig. 10h–l), providing an anatomical basis for the functional differences between these GLP1R-expressing populations. To confirm that AP^{GLP1R} and NTS^{GLP1R} neurons have mostly distinct axon projections, we injected 20 nl of AAV2.2 virus encoding EYFP into the AP or NTS of *Glp1r-ires-Cre* mice. This analysis revealed axon terminals in the lPBN of AP^{GLP1R}-injected mice, and axon terminals in the PVH of NTS^{GLP1R}-injected mice, with almost no collateralization (Fig. 5d,e and Extended Data Fig. 10m–r). Chemogenetic stimulation of AP^{GLP1R} and NTS^{GLP1R} neurons activated neurons in their respective downstream target regions: in the external lPBN, most activated (Fos+, 71%) neurons expressed calcitonin-gene-related peptide (CGRP (Calca); Extended Data Fig. 11a,b); in the PVH, Fos+ cells (42%) expressed the melanocortin 4 receptor (MC4R; Extended Data Fig. 11c). lPBN^{CGRP} neurons suppress food intake and drive aversion[28–30], and PVH^{MC4R} neurons mediate satiety[31–33]. Therefore, AP^{GLP1R} and NTS^{GLP1R} neurons send projections to largely different downstream brain regions and cell types to potentially mediate distinct anorexic behaviours.

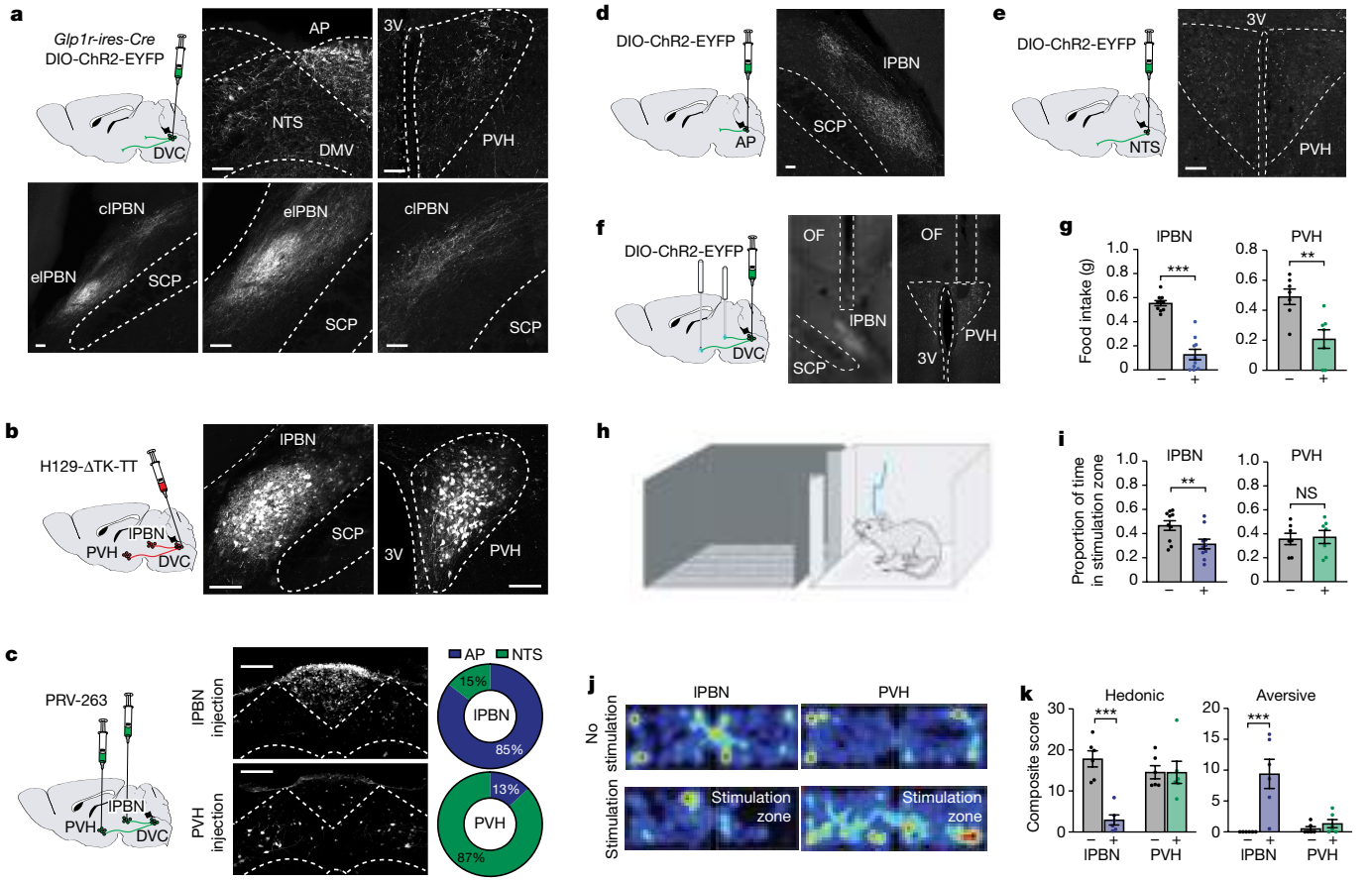

Fig. 5 | AP^{GLP1R} and NTS^{GLP1R} neurons form discrete projections to mediate functionally dissociable behaviours. a, ChR2-DIO-EYFP was injected into the DVC of *Glp1r-ires-Cre* mice (left, schematic). Representative images of: injection site (top middle); axons in the PVH (top right) and in the lPBN (bottom row) ($n = 3$ mice). Scale bars, 50 µm. elPBN, external lPBN; clPBN, central lPBN; SCP, superior cerebellar peduncle. **b**, Cre-dependent H129-ΔTK-TT was injected into the DVC (left, schematic). Representative images of anterogradely labelled neurons in the lPBN (middle) and PVH (right) 2 days after the injection ($n = 3$ mice). Scale bar, 50 µm. **c**, The lPBN or PVH was injected with PRV-263, which expresses EYFP/mCerulean in retrogradely transported GLP1R neurons (schematic). Representative images of AP (top middle) or NTS (bottom middle) EYFP/mCerulean-expressing neurons that project to the lPBN and PVH, respectively. Scale bar, 100 µm. Right, quantification of retrogradely labelled EYFP/mCerulean neurons in AP and NTS from injection in the lPBN or PVH ($n = 3$ mice per group). **d**, AAV2.2-DIO-ChR2-EYFP was injected into the AP (left, schematic). Representative image of axons in the lPBN (right) ($n = 3$ mice). Scale bar, 50 µm. **e**, AAV2.2-DIO-ChR2-EYFP was injected into the NTS (left, schematic). Representative image of axons in the PVH (right) ($n = 3$ mice). Scale bar, 50 µm. **f**, Schematic (left) and representative images of optic fibre (OF) placement above the lPBN (middle) and PVH (right) for axonal stimulation of DVC^{GLP1R} neuron axon projections. **g**, Food intake in fasted mice with optogenetic stimulation of DVC^{GLP1R} axons in the lPBN (left; $n = 10$ mice, two-sided paired *t*-test, no stimulation (−) versus stimulation (+), $P < 0.001$) or PVH (right; $n = 7$ mice, two-sided paired *t*-test, no stimulation (−) versus stimulation (+), $P < 0.01$). **h**, Schematic for real-time place-avoidance assay. The blue fibre represents optogenetic stimulation. **i**, Proportion of time spent in the stimulation zone for mice with optogenetic stimulation of DVC^{GLP1R} axons in the lPBN (left; $n = 10$ mice, paired *t*-test, $P < 0.01$) or PVH (right; $n = 7$ mice, paired *t*-test, NS). **j**, Representative heat maps of time spent in real-time place-avoidance apparatus. **k**, Composite score of hedonic (left; $n = 6$ mice per group, two-way ANOVA, lPBN no stimulation (−) versus stimulation (+), $P < 0.001$; PVH no stimulation (−) versus stimulation (+), NS) and aversive (right; $n = 6$ mice per group, two-way ANOVA, lPBN no stimulation (−) versus stimulation (+), $P < 0.001$; PVH no stimulation (−) versus stimulation (+), NS) real-time taste reactivity responses. Values are mean ± s.e.m. $^*P < 0.05$, $^{**}P < 0.01$, $^{***}P < 0.001$.

To test the functional relevance of these divergent GLP1R projections, we injected *Glp1r-ires-Cre* mice in the DVC with a Cre-dependent virus expressing channelrhodopsin-2 (ChR2) or a control (EYFP), and implanted optic fibres above either the lPBN or the PVH (Fig. 5f). Activation of either AP^{GLP1R} neurons that project to the lPBN (AP^{GLP1R}→lPBN neurons) or NTS^{GLP1R} neurons that project to the PVH (NTS^{GLP1R}→PVH neurons) significantly inhibited food intake in ChR2-expressing (Fig. 5g) but not in EYFP-expressing (Extended Data Fig. 12a,b) mice. Taking advantage of the ability to rapidly and reversibly activate neural activity in AP^{GLP1R}→lPBN or NTS^{GLP1R}→PVH neurons, we used a real-time place-avoidance assay to test whether these projections mediate valence (Fig. 5h). Optogenetic activation of AP^{GLP1R}→lPBN neurons, but not of NTS^{GLP1R}→PVH neurons, significantly reduced the time spent in the environment where mice received stimulation (Fig. 5h–j and Extended Data Fig. 12c–j). Similarly, optogenetic activation of AP^{GLP1R}→lPBN, but not of NTS^{GLP1R}→PVH, projections reduced hedonic and increased aversive real-time taste reactivity[34] to the intraoral delivery of a flavour stimulus (Fig. 5k, Extended Data Fig. 6g,h,k,l and Extended Data Fig. 12k–n). Overall, these data highlight NTS^{GLP1R}→PVH neurons as potential neural targets for satiety without aversion.

Discussion

The most promising obesity therapeutics, GLP1R agonists, cause nausea and vomiting, and it remains an open question whether the therapeutic and adverse effects of these drugs can be functionally dissociated. Here, we demonstrate that hindbrain GLP1R neurons are a critical site of action for GLP1-based obesity therapeutics, and we reveal two anatomically and functionally distinct GLP1R projections, arising from the AP and the NTS, that drive aversion and satiety, respectively.

Previous work had identified GLP1R-expressing populations in the AP and the NTS, with recent single-cell transcriptomics studies[13,16,17,35] confirming earlier histological reports[11,12,36,37]. We functionally dissociated AP^{GLP1R} and NTS^{GLP1R} neurons in mice by developing strategies to independently manipulate and monitor in vivo neural activity in these populations. The current findings add to previous studies on hindbrain GLP1R signalling from our group and others[38–42] by highlighting an NTS^{GLP1R}→PVH circuit that suppresses feeding without inducing aversion. This is especially important given recent findings highlighting other NTS cell types, Tac1 (ref. 14) and ADCYAP1 (ref. 43), which are largely distinct from NTS^{GLP1R} neurons, in mediating nausea-like or sickness behaviours. Importantly, we demonstrate that obesity drugs remain effective at inducing satiety even when aversion circuitry is inhibited. This finding aligns with work showing that AP lesion does not block the satiating effects of GLP1R ligands[39,44]. By contrast, our findings challenge previous studies indicating that GLP1-based therapeutics suppress food intake and body weight through action on distributed neural circuits, including the hypothalamus[10,44]. Rather, our data indicate that key drug-accessible GLP1R populations outside the hindbrain (including vagal afferents and the hypothalamus[45]) are dispensable for their therapeutic effects, a notion that is supported by earlier work in decerebrate rats[46]. Similarly, NTS serotonin 2C receptors ($5HT_{2C}R$) are both necessary and sufficient for the anorexic effects of a previously used obesity drug, lorcaserin[47]. These data emphasize the primacy of NTS signalling in the neural control of food intake and body weight, although it is important to note that our findings do not rule out potential smaller contributions of the hypothalamus or other brain regions to the effects of GLP1-based obesity drugs[10,44,48].

We demonstrate that AP^{GLP1R} neurons project to the lPBN to transmit aversion, whereas NTS^{GLP1R} neurons project to the PVH without evoking aversion. Interestingly, NTS^{CCK} neurons also project to the lPBN and PVH, and NTS^{CCK}→lPBN projections cause negative valence but NTS^{CCK}→PVH projections do not[49–51]. Given that a minority of NTS^{GLP1R} neurons express CCK[16] (Extended Data Fig. 8q), this pattern of discrete, functionally dissociable projections within the same cell type may reflect a more general organizational principle across NTS cell types that mediate satiety.

We developed a platform to monitor in vivo calcium dynamics simultaneously in AP^{GLP1R} and NTS^{GLP1R} neurons, and monitored responses to semaglutide as well as to nutritive and nauseogenic/aversive stimuli. These data complement results from papers on the activity dynamics of NTS neurons in response to oral and gut-derived signals[52,53] and, importantly, provide in vivo evidence of hindbrain activation by GLP1-based obesity drugs. Although fluorescently tagged semaglutide binds in both the AP and the NTS[10], further studies are required to determine whether the observed calcium dynamics are a result of direct or indirect action on the recorded neurons.

As well as showing in vivo activation of DVC^{GLP1R} neurons in response to semaglutide, we also demonstrate that DVC^{GLP1R} neurons form at least two subpopulations that are activated by either nutritive or aversive stimuli (and are much less likely to be activated by both). Furthermore, our data reveal differences between AP^{GLP1R} and NTS^{GLP1R} neurons in their overall responsivity to nutritive and aversive stimuli. However, although the behavioural effects of AP^{GLP1R} and NTS^{GLP1R} neuron activation were distinct, the physiological response properties of these populations were mixed in nature. Indeed, although AP^{GLP1R} neurons generally had greater responses to aversive stimuli and NTS^{GLP1R} neurons had greater responses to nutritive stimuli, this neural tuning was not absolute. Although it is possible that these neuron populations filter broader classes of stimuli before exerting effects on behaviour, we think that the mixed nature of the physiological responses is at least in part a result of the mixed nature of the stimuli, with nutritive stimuli perhaps having some aversive properties (especially given the nature of the intraduodenal delivery) and aversive/nauseogenic stimuli having appetite-suppressing properties. We also note that technical constraints, such as imaging under anaesthesia and applying only one trial each of nutritive and aversive stimuli in the same imaging session, limit the interpretation of results. Nonetheless, the consistency in proportional AP^{GLP1R} and NTS^{GLP1R} neural responses to stimuli across mice lend support to the biased tuning of NTS^{GLP1R} neurons to nutritive rather than aversive stimuli.

Clinically, the adverse gastrointestinal side effects of GLP1-based obesity drugs are more severe at the start of treatment and tend to decrease over time[54]. Future experiments are needed to determine the engagement of AP^{GLP1R} and NTS^{GLP1R} neurons across longer periods of obesity-drug treatment, and how this may correlate with feeding and aversive behaviour. Ultimately, our in vivo imaging approach may be used to screen future potential obesity drugs for preferential activation of hindbrain satiety but not aversion circuits.

Our dissection of the neural circuitry mediating the satiety and aversion effects of GLP1-based obesity drugs demonstrates that distinct projections, AP^{GLP1R}→lPBN and NTS^{GLP1R}→PVH neurons, mediate behaviourally distinct anorexic effects. However, the finding that obesity drugs still suppress food intake even in the absence of the aversion pathway emerging from AP^{GLP1R} neurons indicates that the intake-suppressive effects of these projections are not additive. Indeed, activation of AP^{GLP1R} or NTS^{GLP1R} neurons leads to the same magnitude of food intake suppression as activating both (activating all DVC^{GLP1R} neurons). However, it is unclear how these distinct projections ultimately result in non-additive food intake suppression. One possibility is that distinct hindbrain GLP1R projections mediate different aspects of anorexia (nausea/aversion and physiological satiety) but converge on a common central site of integration for feeding behaviour. Another possibility is that neural circuitry engaged by competing drives (such as hunger) modulate activity in either or both of these pathways to prevent additive effects. Indeed, hunger-sensitive AgRP neurons project to both the lPBN and the PVH to modulate feeding behaviour[55,56]. Furthermore, given the role of GLP1R signalling in reducing motivational aspects of feeding and other behaviours such as alcohol and drug intake[38,57–59], it is also likely that one or both of these DVC^{GLP1R} projections ultimately engages motivation or reward circuitry.

More broadly, this study demonstrates that functionally dissociable neural circuits mediate different effects of the same drug. Because nausea and vomiting are side effects of thousands of treatments for human disease[60], this concept could be applied to investigate therapeutics beyond those used for obesity, with the goal of developing drugs that better target mechanisms that eliminate pathologies and alleviate disease symptoms but avoid negative side effects.

Online content

Any methods, additional references, Nature Portfolio reporting summaries, source data, extended data, supplementary information, acknowledgements, peer review information; details of author contributions and competing interests; and statements of data and code availability are available at https://doi.org/10.1038/s41586-024-07685-6.

1. Wadden, T. A. et al. Effect of subcutaneous semaglutide vs placebo as an adjunct to intensive behavioral therapy on body weight in adults with overweight or obesity: The STEP 3 Randomized Clinical Trial. *JAMA* **325**, 1403–1413 (2021).
2. Wilding, J. P. H. et al. Once-weekly semaglutide in adults with overweight or obesity. *N. Engl. J. Med.* **384**, 989–1002 (2021).
3. World Obesity Federation. *World Obesity Atlas 2023* (World Obesity Federation, 2023).
4. Jastreboff, A. M. et al. Triple-hormone-receptor agonist retatrutide for obesity — a phase 2 trial. *N. Engl. J. Med.* **389**, 514–526 (2023).
5. Jastreboff, A. M. et al. Tirzepatide once Wweekly for the treatment of obesity. *N. Engl. J. Med.* **387**, 205–216 (2022).
6. Muller, T. D. et al. Glucagon-like peptide 1 (GLP-1). *Mol. Metab.* **30**, 72–130 (2019).
7. Hayes, M. R., De Jonghe, B. C. & Kanoski, S. E. Role of the glucagon-like-peptide-1 receptor in the control of energy balance. *Physiol. Behav.* **100**, 503–510 (2010).
8. Krieger, J.-P. et al. Knockdown of GLP-1 receptors in vagal afferents affects normal food iIntake and glycemia. *Diabetes* **65**, 34–43 (2016).

9. Kanoski, S. E., Fortin, S. M., Arnold, M., Grill, H. J. & Hayes, M. R. Peripheral and central GLP-1 receptor populations mediate the anorectic effects of peripherally administered GLP-1 receptor agonists, liraglutide and exendin-4. *Endocrinology* **152**, 3103–3112 (2011).
10. Gabery, S. et al. Semaglutide lowers body weight in rodents via distributed neural pathways. *JCI Insight* **5**, https://doi.org/10.1172/jci.insight.133429 (2020).
11. Jensen, C. B. et al. Characterization of the glucagonlike peptide-1 receptor in male mouse brain using a novel antibody and in situ hybridization. *Endocrinology* **159**, 665–675 (2018).
12. Merchenthaler, I., Lane, M. & Shughrue, P. Distribution of pre-pro-glucagon and glucagon-like peptide-1 receptor messenger RNAs in the rat central nervous system. *J. Comp. Neurol.* **403**, 261–280 (1999).
13. Zhang, C. et al. Area postrema cell types that mediate nausea-associated behaviors. *Neuron* **109**, 461–472 (2021).
14. Xie, Z. et al. The gut-to-brain axis for toxin-induced defensive responses. *Cell* **185**, 4298–4316 (2022).
15. Grill, H. J. & Hayes, M. R. Hindbrain neurons as an essential hub in the neuroanatomically distributed control of energy balance. *Cell Metab.* **16**, 296–309 (2012).
16. Ludwig, M. Q. et al. A genetic map of the mouse dorsal vagal complex and its role in obesity. *Nat. Metab.* **3**, 530–545 (2021).
17. Adriaenssens, A. et al. Hypothalamic and brainstem glucose-dependent insulinotropic polypeptide receptor neurons employ distinct mechanisms to affect feeding. **8**, https://doi.org/10.1172/jci.insight.164921 (2023).
18. Lindberg, J. S. et al. Cinacalcet HCl, an oral calcimimetic agent for the treatment of secondary hyperparathyroidism in hemodialysis and peritoneal dialysis: a randomized, double-blind, multicenter study. *J. Am. Soc. Nephrol.* **16**, 800–807 (2005).
19. Harrington, P. E. & Fotsch, C. Calcium sensing receptor activators: calcimimetics. *Curr. Med. Chem.* **14**, 3027–3034 (2007).
20. Kanoski, S. E., Rupprecht, L. E., Fortin, S. M., De Jonghe, B. C. & Hayes, M. R. The role of nausea in food intake and body weight suppression by peripheral GLP-1 receptor agonists, exendin-4 and liraglutide. *Neuropharmacology* **62**, 1916–1927 (2012).
21. Pelchat, M. L., Grill, H. J., Rozin, P. & Jacobs, J. Quality of acquired responses to tastes by *Rattus norvegicus* depends on type of associated discomfort. *J. Comp. Psychol.* **97**, 140–153 (1983).
22. Grill, H. J. & Norgren, R. The taste reactivity test. I. Mimetic responses to gustatory stimuli in neurologically normal rats. *Brain Res.* **143**, 263–279 (1978).
23. Watakabe, A. et al. Comparative analyses of adeno-associated viral vector serotypes 1, 2, 5, 8 and 9 in marmoset, mouse and macaque cerebral cortex. *Neurosci. Res.* **93**, 144–157 (2015).
24. Wilson-Pérez, H. E. et al. Vertical sleeve gastrectomy is effective in two genetic mouse models of glucagon-like Peptide 1 receptor deficiency. *Diabetes* **62**, 2380–2385 (2013).
25. Murphy, S. et al. Nucleus of the solitary tract A2 neurons control feeding behaviors via projections to the paraventricular hypothalamus. *Neuropsychopharmacology* **48**, 351–361 (2023).
26. Rinaman, L. Ascending projections from the caudal visceral nucleus of the solitary tract to brain regions involved in food intake and energy expenditure. *Brain Res.* **1350**, 18–34 (2010).
27. Wang, D. et al. Whole-brain mapping of the direct inputs and axonal projections of POMC and AgRP neurons. *Front. Neuroanat.* **9**, 40 (2015).
28. Carter, M. E., Han, S. & Palmiter, R. D. Parabrachial calcitonin gene-related peptide neurons mediate conditioned taste aversion. *J. Neurosci.* **35**, 4582–4586 (2015).
29. Campos, C. A., Bowen, A. J., Schwartz, M. W. & Palmiter, R. D. Parabrachial CGRP neurons control meal termination. *Cell Metab* **23**, 811–820 (2016).
30. Carter, M. E., Soden, M. E., Zweifel, L. S. & Palmiter, R. D. Genetic identification of a neural circuit that suppresses appetite. *Nature* **503**, 111–114 (2013).
31. Li, M. M. et al. The paraventricular hypothalamus regulates satiety and prevents obesity via two genetically distinct circuits. *Neuron* **102**, 653–667 (2019).
32. Zhang, S. X. et al. Competition between stochastic neuropeptide signals calibrates the rate of satiation. Preprint at *bioRxiv* https://doi.org/10.1101/2023.07.11.548551 (2023).
33. Fenselau, H. et al. A rapidly acting glutamatergic ARC→PVH satiety circuit postsynaptically regulated by α-MSH. *Nat. Neurosci.* **20**, 42–51 (2017).
34. Spector, A. C., Breslin, P. & Grill, H. J. Taste reactivity as a dependent measure of the rapid formation of conditioned taste aversion: a tool for the neural analysis of taste-visceral associations. *Behav. Neurosci.* **102**, 942–952 (1988).
35. Dowsett, G. K. C. et al. A survey of the mouse hindbrain in the fed and fasted states using single-nucleus RNA sequencing. *Mol Metab* **53**, 101240 (2021).
36. Cork, S. C. et al. Distribution and characterisation of Glucagon-like peptide-1 receptor expressing cells in the mouse brain. *Mol. Metab.* **4**, 718–731 (2015).
37. Göke, R., Larsen, P. J., Mikkelsen, J. D. & Sheikh, S. P. Distribution of GLP-1 binding sites in the rat brain: evidence that exendin-4 is a ligand of brain GLP-1 binding sites. *Eur. J. Neurosci.* **7**, 2294–2300 (1995).
38. Alhadeff, A. L. & Grill, H. J. Hindbrain nucleus tractus solitarius glucagon-like peptide-1 receptor signaling reduces appetitive and motivational aspects of feeding. *Am. J. Physiol. Regul. Integr. Comp. Physiol.* **307**, R465–R470 (2014).
39. Fortin, S. M. GABA neurons in the nucleus tractus solitarius express GLP-1 receptors and mediate anorectic effects of liraglutide in rats., *Sci. Transl. Med.* **12**, eaay8071 (2020).
40. Hayes, M. R. et al. Intracellular signals mediating the food intake-suppressive effects of hindbrain glucagon-like peptide-1 receptor activation. *Cell Metab.* **13**, 320–330 (2011).
41. Alhadeff, A. L. et al. Endogenous glucagon-like peptide-1 receptor signaling in the nucleus tractus solitarius is required for food intake control. *Neuropsychopharmacology* **42**, 1471–1479 (2017).
42. Costa, A. et al. Anorectic and aversive effects of GLP-1 receptor agonism are mediated by brainstem cholecystokinin neurons, and modulated by GIP receptor activation. *Mol. Metab.* **55**, 101407 (2022).
43. Ilanges, A. et al. Brainstem ADCYAP1^{+} neurons control multiple aspects of sickness behaviour. *Nature* **609**, 761–771 (2022).
44. Secher, A. et al. The arcuate nucleus mediates GLP-1 receptor agonist liraglutide-dependent weight loss. *J. Clin. Invest.* **124**, 4473–4488 (2014).
45. Burmeister, M. A. et al. The hypothalamic glucagon-like peptide 1 receptor Is sufficient but not necessary for the regulation of energy balance and glucose homeostasis in mice. *Diabetes* **66**, 372–384 (2017).
46. Hayes, M. R., Skibicka, K. P. & Grill, H. J. Caudal brainstem processing is sufficient for behavioral, sympathetic, and parasympathetic responses driven by peripheral and hindbrain glucagon-like-peptide-1 receptor stimulation. *Endocrinology* **149**, 4059–4068 (2008).
47. D'Agostino, G. et al. Nucleus of the solitary tract serotonin 5-HT_{2C} receptors modulate food intake. *Cell Metab.* **28**, 619–630 (2018).
48. Webster, A. N. et al. Molecular connectomics reveals a glucagon-like peptide 1 sensitive neural circuit for satiety. Preprint at *bioRxiv* https://doi.org/10.1101/2023.10.31.564990 (2023).
49. D'Agostino, G. et al. Appetite controlled by a cholecystokinin nucleus of the solitary tract to hypothalamus neurocircuit., *eLife* **5**, e12225 (2016).
50. Roman, C. W., Sloat, S. R. & Palmiter, R. D. A tale of two circuits: CCK^{NTS} neuron stimulation controls appetite and induces opposing motivational states by projections to distinct brain regions. *Neuroscience* **358**, 316–324 (2017).
51. Cheng, W. et al. Calcitonin receptor neurons in the mouse nucleus tractus solitarius control energy balance via the non-aversive suppression of feeding. *Cell Metab.* **31**, 301–312 (2020).
52. Ran, C., Boettcher, J. C., Kaye, J. A., Gallori, C. E. & Liberles, S. D. A brainstem map for visceral sensations. *Nature* **609**, 320–326 (2022).
53. Ly, T. et al. Sequential appetite suppression by oral and visceral feedback to the brainstem. *Nature* **624**, 130–137 (2023).
54. Shu, Y. et al. Gastrointestinal adverse events associated with semaglutide: a pharmacovigilance study based on FDA adverse event reporting system. *Front. Public Health* **10**, 996179 (2022).
55. Atasoy, D., Betley, J. N., Su, H. H. & Sternson, S. M. Deconstruction of a neural circuit for hunger. *Nature* **488**, 172–177 (2012).
56. Wu, Q., Boyle, M. P. & Palmiter, R. D. Loss of GABAergic signaling by AgRP neurons to the parabrachial nucleus leads to starvation. *Cell* **137**, 1225–1234 (2009).
57. Egecioglu, E. et al. The glucagon-like peptide 1 analogue Exendin-4 attenuates alcohol mediated behaviors in rodents. *Psychoneuroendocrinology* **38**, 1259–1270 (2013).
58. Tuesta, L. M. et al. GLP-1 acts on habenular avoidance circuits to control nicotine intake. *Nat. Neurosci.* **20**, 708–716 (2017).
59. Schmidt, H. D. et al. Glucagon-like peptide-1 receptor activation in the ventral tegmental area decreases the reinforcing efficacy of cocaine. *Neuropsychopharmacology* **41**, 1917–1928 (2016).
60. Wickham, R. J. Nausea and vomiting: a palliative care imperative. *Curr. Oncol. Rep.* **22**, 1 (2020).

Methods

Drug and reagents

Paraformaldehyde (PFA; 441244), bovine serum albumin (A7906), Triton X-100 (T8787), dimethyl sulfoxide (DMSO, D8418), 2,2-thiodiethanol (166782), cinacalcet (SML2012), lithium chloride (L9650), saccharin (240931) and fast green FCF (68724) were purchased from Millipore Sigma. Phosphate buffered saline (SH30013.04) was purchased from Cytiva. Fluoro-Gel (17985) was purchased from Electron Microscopy Science. CNO (4936), RNAscope Multiplex Fluorescent V2 Assay (323100) and RNAscope probes were purchased from Bio-Techne. Exendin-4 (H8730) was purchased from Bachem. Semaglutide (29969) was purchased from Cayman.

Adenoassociated viral vectors

AAV5-EF1a-DIO-taCasp3-TEVp (45580-AAV5), AAV5-syn-DIO-hM3Dq-mCherry (44361-AAV5), AAV5-syn-DIO-EGFP (50457-AAV5), AAV2-syn-DIO-hM3Dq-mCherry (44361-AAV2), AAV2-syn-DIO-hM4Di-mCherry (44362-AAV2), AAV5-EF1a-DIO-hChR2(H134R)-EYFP (20298-AAV5), AAV5-EF1a-DIO-EYFP (27056-AAV5), AAV1-syn-DIO-GCamP6s (100845-AAV1), AAV2-syn-Cre-P2A-dTomato (107738-AAV2) and AAV5-EF1a-DIO-EGFPL10a (98747) were purchased from Addgene. AAV9-EF1a-DIO-DTA (v62-9) and AAV2/2-hER1a-DIO-hChR2(H134R)-EYFP (v214-2) were purchased from the viral vector facility (VVF) of the Neuroscience Center Zurich. AAVDJ8-EF1a-DIO-NaChBac-EGFP was a gift from B. Arenkiel (Baylor College of Medicine). Herpes simplex virus type 1 (H129-ΔTK-TT) and PRV-263 were purchased from the Center for Neuroanatomy with Neurotropic Viruses (CNNV, funded by NIH P40 OD01096).

Mice

Glp1r-ires-Cre (029283, Glp1r$^{tm1.1(cre)Lbrl}$/RcngJ)[61], *Ai9* (007909, B6.Cg-Gt(ROSA)26Sor$^{tm9(CAG-tdTomato)Hze}$/J)[62], *Glp1rtm1Ssis* (Glp1r$^{fl/fl}$, 5637837, a gift from R. Seeley)[24] and C57BL/6 J (WT, 000664) were used in experiments. All mice (except *Glp1rtm1Ssis*) were obtained from Jackson Labs and bred for experiments. Mice were group housed (a maximum of five mice per cage) on a 12 h:12 h light:dark cycle at 22 °C with ad libitum access to rodent chow (5001, LabDiet) and water, unless otherwise noted. Humidity was maintained on average at 55%. Adult male and female mice (at least 8 weeks old) were used for experimentation, except for one experiment (Fig. 1e) in which only males were used, to avoid the confounding variable of time after neural ablation, because our female mice did not achieve diet-induced obesity with 8 weeks of the high-fat diet[63]. Power analyses were run (beta = 0.2 (80% power), alpha = 0.05) with effect sizes based on pilot studies (n = 3–6) to ensure that sample sizes (number of mice for behavioural studies, number of neurons for physiological and anatomical studies) were sufficient to determine significant differences between groups. On the basis of these results, we repeated experiments in an extra cohort (or cohorts) of mice. For in vivo imaging we used 5–7 mice, and for ex vivo anatomical experiments we analysed three brain sections per mouse from at least three mice per group, which are standard sample sizes for imaging and anatomical studies in neuroscience. Investigators collecting (performing behavioural measurements, for example) or analysing (counting neurons, for example) data were blinded to experimental conditions. Apart from one experiment (Extended Data Fig. 1f) that had a smaller but still significant effect in female compared with male mice, we did not observe any significant sex differences across all studies; therefore, we combined results for males and females. All mice were habituated to handling and experimental conditions before experimentation. For within-subject behavioural analyses, all mice received all experimental conditions. For between-subject analyses, mice were randomly assigned to experimental conditions. There were no exclusions from the studies apart from the following. For food intake measurements, mice with considerable spillage were excluded from analysis (n = 3 from DVC NaChBac studies, n = 5 from Casp3/DTA/control ablation studies and n = 3 from GLP1R deletion studies). For neural ablation experiments (across several cohorts of five experimental groups of mice), n = 4 mice were excluded because of unexpected illness and euthanasia during experimentation. For meal-pattern analyses, mice with no food intake were excluded from inter-meal interval analyses (n = 2 mice in AP^{GLP1R} versus NTS^{GLP1R} chemogenetic stimulation experiments). Across all taste reactivity experiments, n = 1 mouse was excluded for a strong aversive response at baseline. For real-time place-preference studies, n = 3 data points were excluded because of mice escaping from the apparatus. Where appropriate, viral expression was verified post mortem, and any mouse that did not express virus or expressed virus outside the target region was excluded from analyses. All the NS results reported throughout the manuscript are biological replicates. All procedures were approved by the Monell Chemical Senses Center Institutional Animal Care and Use Committee.

Surgery

Mice were anaesthetized with inhaled isoflurane (1–2%) and received bupivacaine (2 mg per kg, subcutaneous) at the site of surgical incision and meloxicam (5 mg per kg, subcutaneous) analgesia once daily for 3 days after surgery. All mice were given at least two weeks for recovery before experimentation unless otherwise noted.

Viral injections and optical fibre implantation. All mice that received surgery were *Glp1r-ires-Cre* mice except where noted. Viral expression specifically in GLP1R neurons was validated using in situ hybridization (Extended Data Fig. 1a).

Mice received viral injections with or without optical fibre implantation with methods similar to those we have previously published[64,65]. In brief, mice were anaesthetized and placed in a stereotaxic frame. For central GLP1R neuron ablation, 100 nl AAV5-EF1a-DIO-taCasp3-TEVp was injected into the DVC (0.45 mm anterior, ±0.15 mm lateral, 0.18 mm ventral from the obex) or the ARC (1.35 mm posterior, ±0.25 mm lateral, 6.15 mm ventral from bregma). For ablation of GLP1R neurons in the NG, we injected AAV9-EF1a-DIO-DTA with 0.05% Fast Green FCF. Genes carried by the AAV5 serotype do not transfect in NG neurons. Because there is no available packaged Caspase with the AAV9 serotype (which works well in NG neurons), and because DTA has been used previously to ablate NG neurons[66], we used a different virus (AAV9-EF1a-DIO-DTA) than that used in the ARC and DVC to ablate NG^{GLP1R} neurons. For NG injection, an incision was made in the neck and the sternohyoid and sternomastoid muscle connective tissue was blunt dissected and moved aside to expose the carotid artery. The vagus nerve was gently separated and followed to reach the nodose ganglion as it enters the foramen. A glass micropipette was advanced into the ganglion and the virus was injected. The procedure was repeated on the contralateral ganglion. We verified that both techniques (Casp3 and DTA) effectively ablated the neurons of interest (Extended Data Fig. 1b,c). For chemogenetic activation studies, 100 nl AAV5-syn-DIO-hM3D-mCherry or AAV5-syn-DIO-EGFP was injected in the DVC, 20 nl of AAV2-syn-DIO-hM3D-mCherry was injected in the AP (0.45 mm anterior, 0 mm lateral, 0.16 mm ventral from the obex) or bilaterally in the NTS (0.45 mm anterior, ±0.30 mm lateral, 0.2 mm ventral from the obex). For chronic neural activation studies, 100 nl AAVDJ8-EF1a-DIO-NaChBac-EGFP or AAV5-syn-DIO-EGFP was bilaterally injected in the DVC. To knock out the GLP1R, 100 nl AAV2-syn-Cre-P2A-dTomato was bilaterally injected in the DVC, or 20 nl of the vector was injected in the AP or bilaterally in the NTS, of *Glp1r$^{fl/fl}$* or control C57BL/6 J mice. For quantification of DVC^{GLP1R} neurons, and for whole-mount tissue confocal imaging, 100 nl AAV5-EF1a-DIO-EGFPL10a was bilaterally injected in the DVC. For optogenetic activation and optical fibre implantation, 100 nl AAV5-EF1a-DIO-hChR2(H134R)-EYFP or AAV5-EF1a-DIO-EYFP was injected in the DVC. A 200-µm optical fibre (FT200UMT, Thorlabs) was placed above either the lPBN

(1.30 mm posterior, 1.60 mm lateral, 3.40 mm ventral from lambda) or PVH (0.60 mm posterior, 0.25 mm lateral, 4.8 mm ventral from bregma) and secured to the skull with dental cement. For in vivo calcium imaging, 150 nl AAV1-syn-DIO-GCamP6s was injected in the DVC (0.25 mm anterior, ±0.15 mm lateral, 4.15 mm ventral from the occipital suture) of *Glp1r-ires-Cre*;*Ai9* mice. For anterograde tracing, 100 nl HSV H129-ΔTK-TT (5×10^8 vg ml^{-1}) was bilaterally injected in the DVC, and brains were collected 24 h and 48 h after injection. To anterogradely trace the projections of AP^{GLP1R} or NTS^{GLP1R} neurons, 20 nl AAV-2/2-hER1a-DIO-hChR2(H134R)-EYFP was injected in the AP or bilaterally in the NTS and brains were collected two weeks after injection. For retrograde tracing, 150 nl PRV-263 (1×10^9 vg ml^{-1}) was injected in either the lPBN (1.30 mm posterior, ±1.60 mm lateral, 3.60 mm ventral from lambda) or PVH (0.60 mm posterior, ±0.25 mm lateral, 4.95 mm ventral from bregma), and brains were collected 36 h after injection.

Intraoral cannula surgery. Mice were implanted with a unilateral intraoral cannula consisting of polyethylene tubing (PE50CL100, Braintree Scientific), heat-flared to hold a Teflon washer (5612-120-25, Seastrom) on the proximal end and press fit with 23 G stainless-steel tubing on the distal end. The cannulae were implanted inside the cheek, just lateral to the first maxillary molar, as previously described in rats[67]. The distal end of the catheter was secured to the skull with dental cement. Mice received moistened chow for two days after surgery before returning to maintenance on regular chow.

Immunohistochemistry, in situ hybridization and imaging

Mice were transcardially perfused with PBS followed by 4% PFA, and brains were collected and post-fixed overnight in PFA. Brains were coronally sectioned (16–150 µm) on a vibratome or cryostat. For immunohistochemistry, brain sections were incubated with primary antibodies in 1% bovine serum albumin and 0.1% Triton X-100 in PBS overnight at 4 °C. On the second day, brain sections were washed with PBS three times, followed by incubation with secondary antibodies for 1 h at room temperature. Brain sections were washed with PBS three times, mounted on slides and coverslipped with Fluoro-Gel. Antibodies used were sheep anti-EGFP (1:1000, 4745-1051, Bio-Rad), rabbit anti-RFP (1:1000, 600-401-379, Rockland), donkey anti-sheep IgG Alex488 (1:500, 713-545-147, Jackson ImmunoResearch) and donkey goat anti-rabbit IgG Cy3 (1:500, 711-165-152, Jackson ImmunoResearch). For in situ hybridization, RNAscope Multiplex Fluorescent V2 Assay was performed, based on the manufacturer's protocol. In brief, brain sections were pretreated with 4% PFA, an ethanol gradient and protease III. Nodose ganglia were pretreated with an ethanol gradient and protease IV (20 min at room temperature). Treated sections were hybridized with *Glp1r*, *Calca*, *Mc4r* and/or *Fos* probes (418851-C3, 578771-C1, 319181-C3, and 316921-C2, respectively), followed by amplification and detection reagents. Finally, sections were counterstained with DAPI and mounted on slides with Fluoro-Gel. Epifluorescence images were acquired with a slide scanner (BZ-X800, Keyence) with a 10× objective lens and confocal microscope (Stellaris 5, Leica, purchased with S10OD030354) with a 20× objective lens. Images were analysed (three sections per mouse per experiment) using the spots function in Imaris 9.3 software (Oxford Instruments) to detect positive neurons according to the size and shape of neurons and the image background. We manually marked the subregions of the DVC on the basis of anatomical landmarks using the surface function in Imaris. Colocalization was calculated using the filter function in Imaris.

Whole-mount tissue imaging

Brains were collected and post-fixed overnight in PFA. Brains were washed with PBS and a portion of the cerebellum was removed to expose the medulla. The tissue was incubated in a 2,2-thiodiethanol gradient (10%, 25% and 47% in water) until equilibrium was reached. Cleared tissue was imaged from dorsal to ventral (480 µm) with a two-photon microscope (Ultima 2Pplus, Bruker) with a water-immersion objective lens (XLSLPLN25XSVMP2, Evident Scientific). Fluorophore-expressing neurons were detected with the spots function, and the 3D structure was constructed using Imaris 9.3 software.

Experiments using GLP1R agonists

Effects of GLP1R neuron ablation on exendin-4-induced anorexia. Mice were fasted overnight and injected intraperitoneally with saline or 5, 10 or 20 µg per kg exendin-4. Then, 15 min after the injection, mice were given to access to food, and food intake was measured at 0.5, 1, 2, 4 and 8 h.

Effects of GLP1R neuron ablation on semaglutide-induced anorexia. Mice were fasted overnight and injected subcutaneously with vehicle (0.25% DMSO in saline) or 10 µg per kg semaglutide. Then, 4 h after injection, mice were given to access to food, and food intake was measured 4 h later.

Effects of GLP1R neuron inhibition on exendin-4-induced anorexia. Mice were fasted overnight and injected intraperitoneally with vehicle or 1 mg per kg CNO. Then, 15 min after the first injection, mice were injected intraperitoneally with saline or 20 µg per kg exendin-4. Then, 15 min after the second injection, mice were given access to food, and food intake was measured at 0.5, 1, 2, 4 and 8 h.

Effects of GLP1R neuron ablation on semaglutide-induced prevention of weight gain. Mice were maintained on a 60% high-fat diet and received bi-weekly subcutaneous injections of 12 µg per kg semaglutide. Weekly body mass, food intake and body composition (measured by magnetic resonance, minispec, Bruker) were measured.

Effects of GLP1R neuron ablation on semaglutide-induced weight loss. Mice were maintained on a 60% high-fat diet (D12492, Research Diets) for eight weeks, followed by subcutaneous injection of 40 µg per kg semaglutide every two days for one week and daily for the next two weeks. Body mass was measured daily.

Taste reactivity assay

Orofacial taste reactivity tests[22] were modified versions of our protocol in rats[67]. A mirror was mounted under a chamber with a clear Plexiglass floor at an angle of approximately 45°, and a digital video camera (Panasonic X1500 4 K) was positioned facing the mirror on a tripod about 35 cm away to capture food-evoked taste reactivity behaviours. Low-sodium chicken broth (50%, Pacific food) or saccharin (0.05%) was used as a novel flavour and was infused (50 µl) by intraoral cannula at a rate of 0.1 ml min^{-1}. Each infusion was separated by 10–30 s. Mice were naive to the flavour on the first day. Taste-reactivity habituation and testing were done in a cylindrical chamber with clear Plexiglas walls and floor.

Video files were viewed offline using iMovie v.10.2.2 and were slowed to 25% of the original speed for analysis. Responses were categorized into two affective reaction patterns: hedonic reactions and disgust–aversive reactions[22] (Extended Data Fig. 6 and Supplementary Video 3). Hedonic reactions included rhythmic mouth movements (including rhythmic tongue protrusions), lateral tongue protrusions and paw licks. Aversive reactions included gapes, chin rubs and facilitated fluid rejection (including face washing and forelimb flails with ejection of fluid). To give approximately equal weight to all taste reactivity responses, we counted the number of gapes, chin rubs and lateral tongue protrusions, and the remaining continuous responses were quantified in time bins. Specifically, we measured the time (in seconds) spent engaging in rhythmic mouth movements, paw licks and facilitated fluid rejection, and to weight these equally with the other behaviours, we normalized each by a factor of 0.8. The composite score was calculated by summing all of the resulting measures[68,69].

Quinine-induced taste reactivity. Mice received an intraoral infusion of water, 2.4 mM quinine or 4.0 mM quinine in a counterbalanced order. Mice received four intraoral infusions of each stimuli, and video recordings were analysed.

Cinacalcet- or LiCl-induced real-time taste reactivity. To determine whether systemic cinacalcet or LiCl administration causes real-time taste aversion, 5 min before the first intraoral infusion, mice received an intraperitoneal injection of LiCl (6 mmol kg^{-1} in saline) or cinacalcet (15 µmol kg^{-1} in saline with 5% DMSO). Mice received an intraoral infusion every 5 min for the following 30 min. The experiment was run in a within-subject manner in which each mouse received the control and experimental condition paired with either chicken stock or saccharin.

Cinacalcet-induced conditioned taste reactivity. To determine whether cinacalcet produces a conditioned taste aversion, experimental and control mice received eight intraoral infusions of a flavour, followed by intraperitoneal injection of cinacalcet (15 µmol kg^{-1} in saline with 5% DMSO). Three conditioning sessions and one testing session were performed. In between each conditioning session, mice had a 24-h wash-out time, and the testing session was performed 48 h after the last conditioning session. Taste reactivity to the flavour stimulus was recorded and data from the first four infusions from testing (conditioned) sessions were analysed.

LiCl-induced taste reactivity. To determine whether LiCl produces a conditioned taste aversion, experimental and control mice received eight intraoral infusions of a flavour, followed by intraperitoneal injection of LiCl (6 mmol kg^{-1} in saline). Two conditioning sessions and one testing session were done, with a 24-h wash-out time between sessions. Taste reactivity to the flavour stimulus was recorded and data from the first four infusions from testing (conditioned) sessions were analysed.

Chemogenetic GLP1R neuron activation-induced conditioned taste reactivity. To determine whether DVC^{GLP1R}, AP^{GLP1R} or NTS^{GLP1R} neuron activation conditions taste aversion, experimental and control mice received eight intraoral infusions of flavour, followed by intraperitoneal injection of 1 mg kg^{-1} CNO. We waited 24 h between taste-reactivity sessions to wash out the effects of CNO. For each experiment, two or three conditioning sessions and one testing session were done. Taste reactivity to the flavour stimulus was recorded and data from the first four infusions from the baseline and testing (conditioned) sessions were analysed.

Real-time taste reactivity with GLP1R neuron optogenetic stimulation. The axon terminals of DVC^{GLP1R} neurons at the lPBN or the PVH were unilaterally optogenetically stimulated in experimental and control mice with 10-ms pulses (20 mW, 30 Hz, 1.5 s on, 0.5 s off)[50] while mice received eight intraoral infusions of the novel flavour. Data from the last four intraoral infusions (during stimulation) were analysed. Detailed methods for optogenetic stimulation are given below.

CFA assays

CFA by chemogenetic activation of GLP1R neurons. Mice with excitatory chemogenetic receptors in DVC^{GLP1R}, AP^{GLP1R} or NTS^{GLP1R} neurons, or control mice, were housed singly and acclimated to the testing chamber with 19-h water deprivation for three days. To condition the flavour to GLP1R neuron activation, water-deprived mice were allowed to drink 50% chicken broth for 20 min followed by intraperitoneal injection of 1 mg per kg CNO for two conditioning days. On the test day, 20-min chicken broth intake was measured.

Effect of chemogenetic inhibition on semaglutide-induced CFA. Mice were housed singly and acclimated to the testing chamber with 19-h water deprivation for three days. Water-deprived mice were allowed to drink 50% chicken broth followed by intraperitoneal injection of 1 mg per kg CNO. Then, 15 min after the injection of CNO, mice were injected subcutaneously with 120 µg/kg semaglutide. To maintain the suppression of GLP1R neurons for the duration of semaglutide action, mice were intraperitoneally injected with 1 mg per kg CNO every 12 h for two days. After two rounds of conditioning and an extra day for drug wash-out (during which time we verified that mice were no longer losing weight), 20-min chicken broth intake (CFA test) was measured.

Effect of GLP1R deletion on semaglutide-induced CFA. Mice were housed singly and acclimated to the testing chamber with 19-h water deprivation for three days. Water-deprived mice were allowed to drink 50% chicken broth. After 20 min, mice were injected subcutaneously with 120 µg per kg semaglutide. After two rounds of conditioning and an extra day for drug wash-out (during which we verified that mice were no longer losing weight), 20-min chicken broth intake (CFA test) was measured.

In vivo optogenetic stimulation experiments

The output beam from a diode laser (450 nm, Lasever) was controlled by a microcontroller (Arduino Uno) running a pulse-generation script. The laser was coupled to a multimode optical fibre (200 mm core, NA 0.37, Doric) with a 1.25 mm OD zirconium ferrule (Kientech) and mating sleeve that enabled delivery of light to the brain by coupling to the implanted ferrule-capped optical fibre in the mouse.

Effects of optogenetic stimulation of DVC^{GLP1R} projections on food intake. Mice were fasted overnight and axon terminals of DVC^{GLP1R} neurons in the lPBN or PVH (or controls) were optogenetically activated with 10-ms pulses (20 mW, 30 Hz, 1 s on, 4 s off)[49] for 1 h, after which food intake was measured.

Effects of optogenetic stimulation of DVC^{GLP1R} projections on real-time place avoidance. Real-time place avoidance was done in a two-chambered apparatus (ENV-3013, Med Associates) in which one chamber was paired with optogenetic activation (10-ms pulses, 20 mW, 30 Hz, 1.5 s on, 0.5 s off)[50] of DVC^{GLP1R} neurons in the lPBN or PVH (or controls). Mouse position was tracked by the EthoVision XT 16 system (Noldus), which triggered optogenetic stimulation when mice entered the appropriate side of the apparatus. Mice were tested both in the ab libitum and fasted states, with 10 min of no stimulation followed by 20 min with stimulation, repeated for three days[49].

Energy expenditure and meal pattern measurements

Mice were housed individually and acclimated to habituation monitoring chambers for two days before data collection. For chemogenetic activation of DVC^{GLP1R}, AP^{GLP1R} or NTS^{GLP1R} neurons, mice were fasted for 24 h and intraperitoneally injected with 1 mg per kg CNO or vehicle (2% DMSO in saline) at the onset of the dark period. For experiments with chronic DVC^{GLP1R} activation (by NaChBac[70]), mice were fed ad libitum. Food intake, physical activity and O_2/CO_2 exchange were monitored in metabolic chambers (PhenoMaster v5.0.6, TSE systems or Promethion Live v23.0.01, Sable Systems) and data were analysed as previously described[63]. For meal-pattern analyses, a meal was considered to be a bout of food intake of more than 0.02 g. The termination of a meal was determined as more than 10 min with no measurable feeding[63]. Meal patterns were quantified from 4–6 h post-CNO injection, as mice consumed very little food from 0–3 h. Mice that did not eat in this time period ($n = 2$ across all experiments) were excluded from inter-meal interval analyses. Mice with excessive food-grinding behaviours (fewer than 5% of all mice tested) were excluded from all analyses.

In vivo calcium imaging

For in vivo calcium imaging, 150 nl AAV1-syn-DIO-GCamP6s was injected in the DVC (0.25 mm anterior, ±0.15 mm lateral, 4.15 mm ventral from

the occipital suture) of *Glp1r-ires-Cre*;*Ai9(tdTomato)* mice. After four weeks of recovery from stereotaxic surgery, mice were anaesthetized with isoflurane (1–2%) to receive an intravenous catheter, an intraduodenal catheter, an intraduodenal exit port and a cranial window above the DVC. An incision was made in the neck area, and the sternohyoid muscle and fatty tissue were moved aside to expose the jugular vein. The superior end of the jugular vein was ligated and the jugular vein was nicked with 22 G needle. A catheter (C20PU-MJV1458, Instech Laboratories) was inserted into the vein and tied with silk thread. An abdominal midline incision was made to expose the duodenum and stomach, and a duodenal catheter (MRE-033, Braintree Scientific) was inserted through a puncture hole below the pyloric sphincter and secured to the tissue with glue. For the intestinal exit port, the duodenum was truncated around 3 cm below the pyloric sphincter, and the intestinal exit port was left outside the abdominal cavity. Mice were placed on a custom-made platform to bend the head approximately 45° downwards. To expose the obex, a midline incision was made between the ears. The splenius capitis muscle was retracted and the cranial meninges were removed. The skull above the cerebellar lobules was carefully removed using Friedman–Pearson rongeurs (16220-14, Fine Science Tools). To avoid excess bleeding from bone cutting, haemostatic sponges (HY-80208, Hygitech) were applied at the bleeding site as needed. The lobules were pushed rostrally and anchored with a rolled Kimwipe. Artificial cerebrospinal fluid (59-7316, Harvard Apparatus) was applied to avoid drying. We used a stainless-steel column (3 mm in length, 50415K15, McMaster-Carr) attached to a #0 round coverslip (64-0726, Warner Instruments) as a window that we placed on top of the medulla, which we tilted 5–10° downwards along the rostral–caudal axis. This angle enabled simultaneous imaging of the AP and NTS across all *z* planes. To stabilize the window, a custom-made holder attached to a micromanipulator (MX10R, Siskiyou) was attached to the stainless-steel column and gently pressed downwards against the surface of medulla, similar to a previously published approach[52]. To prevent respiratory arrest, blood flow in the vein of the inferior cerebellar peduncle was monitored. The gap between the skull, the window and the custom-made holder was filled with silicone elastomer (KWIK-SIL, World Precision Instruments) and the window was filled with water. The vein of the inferior cerebellar peduncle was used as a landmark to locate the DVC using a microscope (Extended Data Fig. 3f). In vivo calcium images from anaesthetized mice were acquired using a two-photon microscope (Ultima 2Pplus, Bruker) with a water immersion objective lens (XLSLPLN25XSVMP2, Evident Scientific). The laser (Insight X3 Dual, Spectra-Physics) was tuned to 860 nm (for GCaMP6s) and 1,040 nm (for tdTomato, serving as structural channel for data analysis) with 30–60-mW laser power depending on the depth of imaging. Volumetric imaging was done using Optotune ETL (six focal planes 30 µm apart, 1.71 Hz), and this enabled the simultaneous recording of hundreds of DVC^{GLP1R} neurons (215 ± 29 neurons on average per mouse, ranging from 36 to 208 AP^{GLP1R} neurons and 31 to 100 NTS^{GLP1R} neurons per mouse) per imaging session in a field of view of 746.5 × 746.5 µm. Two-photon images were acquired with Prairie View software (v.5.7). To test the effect of semaglutide on DVC^{GLP1R} neuron activity, intravenous infusions were done in two imaging sessions. First, 100 µl vehicle (0.25% DMSO in saline, 0.05 ml min^{-1} intravenous) was infused. Second, 200 µl semaglutide (60 µg per kg, 0.05 ml min^{-1} intravenous) was infused. Baseline recordings were taken for 30 s before each infusion. To determine whether the same cells were responsive to nutritive and aversive stimuli, we imaged neural activity responses to: 300 µl Ensure (66.7%, 0.1 ml min^{-1} intraduodenal, Abbott), 100 µl cinacalcet (0.5 mg per kg, 0.05 ml min^{-1} intravenous, 0.25% DMSO in saline) and 100 µl LiCl (150 mg per kg, 0.05 ml min^{-1} intravenous). Controls for these solutions were: saline infused 0.1 ml min^{-1} intraduodenal and 0.25% DMSO in saline infused 0.05 ml min^{-1} intravenous. Baseline recordings were taken for 60 s before each infusion. Across experiments, imaging was paused between sessions with multiple infusions in the same mice to prevent bleaching artifacts.

Two-photon imaging data were analysed using the CaImAn package (v.1.9.16) in Python (v.3.11.6)[71]. The data were first motion-corrected using a rigid implementation of the NoRMCorre algorithm (v.0.1.1)[72]. The algorithm was run for two iterations on data from a structural channel (Glp1r-tdTomato) and the computed shifts were subsequently applied to the functional channel (GCaMP6s signal). Cellpose (v.2.0.5), a neural-network-based algorithm trained to perform cell segmentation, was then used to identify regions of interest (ROIs) given a maximum projection of the functional channel data along the time axis[73]. Any non-neuronal ROIs were manually discarded. The activity of neurons associated with these ROIs was subsequently extracted using constrained non-negative matrix factorization (CNMF), wherein the ROIs acquired with Cellpose served as seeds for the neuronal spatial components of the model[74]. Calcium transients were modelled with a second-order auto-regressive process with a decay time of approximately 1.8 s to capture GCaMP6s kinetics. Neuropil activity generally manifests in two-photon calcium imaging as less-localized fluctuations in the background fluorescence. If unaccounted for, these background signals could contaminate signals originating from the neurons of interest. Therefore, when fitting the CNMF, two extra spatial components were used to capture any background neuropil activity (the 'nb' parameter for the CNMF in CaImAn). These components usually have spatial footprints that cover a large portion of the field of view because, as previously mentioned, the activity they represent is less localized. The background-subtracted traces for each ROI were normalized by computing *z*-scored activity relative to the mean and standard deviation of data during a 30-s baseline period before the stimulus onset. The ROIs with the median of *z*-scored activity across the stimulation period larger than 1.64 (which is statistically significant at $\alpha = 0.05$ for a one-tailed *z*-test) were considered to be responders[75], and all stimulus-responsive neurons were included in the analyses. Before the analysis of calcium activity (to prevent any bias), boundaries between the AP and NTS were drawn for each z-plane using: first, the differential density of GLP1R neurons in the AP versus the NTS, which creates a natural boundary (density is much higher in the AP than in the NTS; Fig. 2b and Extended Data Fig. 3a,c); and second, the red halo of tdTomato-expressing GLP1R processes that project into the NTS but not into the AP (Extended Data Fig. 3c–e). To display average neural activity responses for each mouse, the previously calculated median *z*-scored activity for each neuron were averaged together and graphed separately for AP^{GLP1R} and NTS^{GLP1R} responses. To visualize differential stimulus preferences for responsive ROIs, we subtracted the median *z*-scores for nutrient responses from the median *z*-scores for aversive stimuli to produce a difference index. These colour-coded 'tuning index' values were mapped to dots at the location of each responsive ROI in Fig. 2l,p and Extended Data Fig. 4e, with the neurons that were more responsive to aversive stimuli depicted in red and the neurons most responsive to nutritive stimuli shown in blue.

For those who wish to adopt this calcium imaging analysis strategy, we point out that there are alternative approaches for motion correction should better frame alignment be necessary. We compared our rigid-body motion-correction method with strategies involving affine (PyStackReg v.0.2.7) and/or piecewise-rigid (the pw-rigid function in NoRMCorre) transformations in Extended Data Fig. 5. Although these corrections did not influence our results or conclusions, they may be necessary for those analysing frames with substantial uniform or non-uniform distortions, especially for preparations with ROIs along image edges.

Transcriptomics

Publicly available transcriptomic data of single cells or nuclei from mouse DVC produced previously[13,16,17] were combined using Seurat (v.4.3.0) in R (v.4.3.0)[76,77]. Count matrices of unique transcripts for each library were normalized individually before dimensionality reduction analysis. Neuronal clusters from each dataset were identified and

placed in subsets on the basis of canonical marker gene expression (*Snap25*, *Syp*, *Rbfox3*, *Mapt*, *Map2*, *Nefl*, *Nefm*, *Nefh*, *Dlg4* and *Syt1*). The resulting neuronal datasets were renormalized individually before merging and integration using canonical correlation analysis followed by mutual nearest-neighbour detection. The integrated dataset was scaled and uniform manifold approximation and projection (UMAP) was generated using the top 30 principal components from principal component analysis. Clustering was done using the Louvain algorithm with a resolution of 1.4. Neuronal clusters were assigned to the AP or the NTS according to the expression patterns of signature genes previously identified[78]. Co-expression of select targets in *Glp1r* neurons was analysed and grouped by region using the Seurat DotPlot function. Data were visualized using ggplot2 (v.3.5.0).

Statistical analyses

All data were expressed as mean ± s.e.m. unless otherwise noted. Paired or unpaired two-tailed *t*-tests, one-way, two-way and repeated-measures ANOVA (with post hoc Bonferroni comparisons), Fisher's exact test and Pearson regression were performed where appropriate using GraphPad Prism (v.10.2.2). Sample sizes, statistical tests and *P*-values for each experiment are listed in Supplementary Table 1. NS, $P > 0.05$; $^{*}P < 0.05$; $^{**}P < 0.01$; $^{***}P < 0.001$.

Reporting summary

Further information on research design is available in the Nature Portfolio Reporting Summary linked to this article.

Data availability

Source data are provided with this paper. Transcriptomic analyses were generated from publicly-accessible data (NCBI GEO databases: GSE160938, GSE166649, GSE228192). Source data are provided with this paper.

Code availability

Custom codes generated to analyse data from the study are accessible at https://github.com/alhadefflab/2p_imaging_analysis.git.

61. Williams, E. K. et al. Sensory neurons that detect stretch and nutrients in the digestive system. *Cell* **166**, 209–221 (2016).
62. Madisen, L. et al. A toolbox of Cre-dependent optogenetic transgenic mice for light-induced activation and silencing. *Nat. Neurosci.* **15**, 793–802 (2012).
63. Huang, K.-P. et al. Sex differences in response to short-term high fat diet in mice. *Physiol. Behav.* **221**, 112894 (2020).
64. Alhadeff, A. L. et al. A neural circuit for the suppression of pain by a competing need state. *Cell* **173**, 140–152 (2018).
65. Goldstein, N. et al. Hypothalamic detection of macronutrients via multiple gut-brain pathways. *Cell Metab.* **33**, 676–687 (2021).
66. Min, S. et al. Arterial baroreceptors sense blood pressure through decorated aortic claws. *Cell Rep.* **29**, 2192–2201 (2019).
67. Ghidewon, M. et al. Growth differentiation factor 15 (GDF15) and semaglutide inhibit food intake and body weight through largely distinct, additive mechanisms. *Diabetes Obes. Metab.* **24**, 1010–1020 (2022).
68. Wyvell, C. L. & Berridge, K. C. Intra-accumbens amphetamine increases the conditioned incentive salience of sucrose reward: enhancement of reward "wanting" without enhanced "liking" or response reinforcement. *J. Neurosci.* **20**, 8122–8130 (2000).
69. Berridge, K. C. & Peciña, S. Benzodiazepines, appetite, and taste palatability. *Neurosci. Biobehav. Rev.* **19**, 121–131 (1995).
70. Ren, D. et al. A prokaryotic voltage-gated sodium channel. *Science* **294**, 2372–2375 (2001).
71. Giovannucci, A. et al. CaImAn an open source tool for scalable calcium imaging data analysis., *eLife* **8**, e38173 (2019).
72. Pnevmatikakis, E. A. & Giovannucci, A. NoRMCorre: an online algorithm for piecewise rigid motion correction of calcium imaging data. *J. Neurosci. Methods* **291**, 83–94 (2017).
73. Stringer, C., Wang, T., Michaelos, M. & Pachitariu, M. Cellpose: a generalist algorithm for cellular segmentation. *Nat. Methods* **18**, 100–106 (2021).
74. Pnevmatikakis, E. A. et al. Simultaneous denoising, deconvolution, and demixing of calcium imaging data. *Neuron* **89**, 285–299 (2016).
75. Tan, H.-E. et al. The gut–brain axis mediates sugar preference. *Nature* **580**, 511–516 (2020).
76. Butler, A., Hoffman, P., Smibert, P., Papalexi, E. & Satija, R. Integrating single-cell transcriptomic data across different conditions, technologies, and species. *Nat. Biotechnol.* **36**, 411–420 (2018).
77. Hao, Y. et al. Integrated analysis of multimodal single-cell data. *Cell* **184**, 3573–3587 (2021).
78. Ludwig, M. Q., Todorov, P. V., Egerod, K. L., Olson, D. P. & Pers, T. H. Single-cell mapping of GLP-1 and GIP receptor expression in the dorsal vagal complex. *Diabetes* **70**, 1945–1955 (2021).

Acknowledgements We thank M. Dietrich and H. Grill for comments on the manuscript; B. Arenkiel and J. Ortiz for providing viral reagents; R. Seeley for providing transgenic mice; P. Bazzino for advice on intraoral catheters; H. Grill for advice on taste-reactivity experiments; C. Ran for advice on two-photon imaging experiments; and Monell Center facilities and administrative staff for animal care and other experimental support. A.L.A. is a New York Stem Cell Foundation Robertson investigator and a Pew biomedical scholar. This work was supported by the National Institutes of Health (R00DK119574 and DP2AT011965 to A.L.A.); the American Heart Association (857082 to A.L.A. and 898990 to K.-P.H.); the New York Stem Cell Foundation (to A.L.A.); the Klingenstein Fund and Simons Foundation (to A.L.A.); the Pew Charitable Trusts (to A.L.A.); the National Science Foundation (2236662 to M.Y.G.); the Penn Institute for Diabetes, Obesity, and Metabolism (to A.L.A.); and the Monell Chemical Senses Center (to K.A.B. and A.L.A.). The confocal microscope used in these studies was purchased with instrumentation grant NIH S10OD030354 (to A.L.A.).

Author contributions K.-P.H., M.Y.G., A.D.M. and A.L.A. conceived and designed the experiments. K.-P.H., A.A.A., M.Y.G., A.D.M., M.S.A., N.T.N., N.D.H., N.P., Y.S.K.G., A.E.A., K.A.B. and A.L.A. performed experiments, analysed data and/or interpreted data; A.L.A. wrote the manuscript with comments from K.-P.H. and all authors.

Competing interests The authors declare that the Monell Chemical Senses Center has filed a patent application related to potential therapeutic compounds.

Additional information

Supplementary information The online version contains supplementary material available at https://doi.org/10.1038/s41586-024-07685-6.

Correspondence and requests for materials should be addressed to Amber L. Alhadeff.

Peer review information *Nature* thanks Mark Andermann, Chuchu Zhang and the other, anonymous, reviewer(s) for their contribution to the peer review of this work.

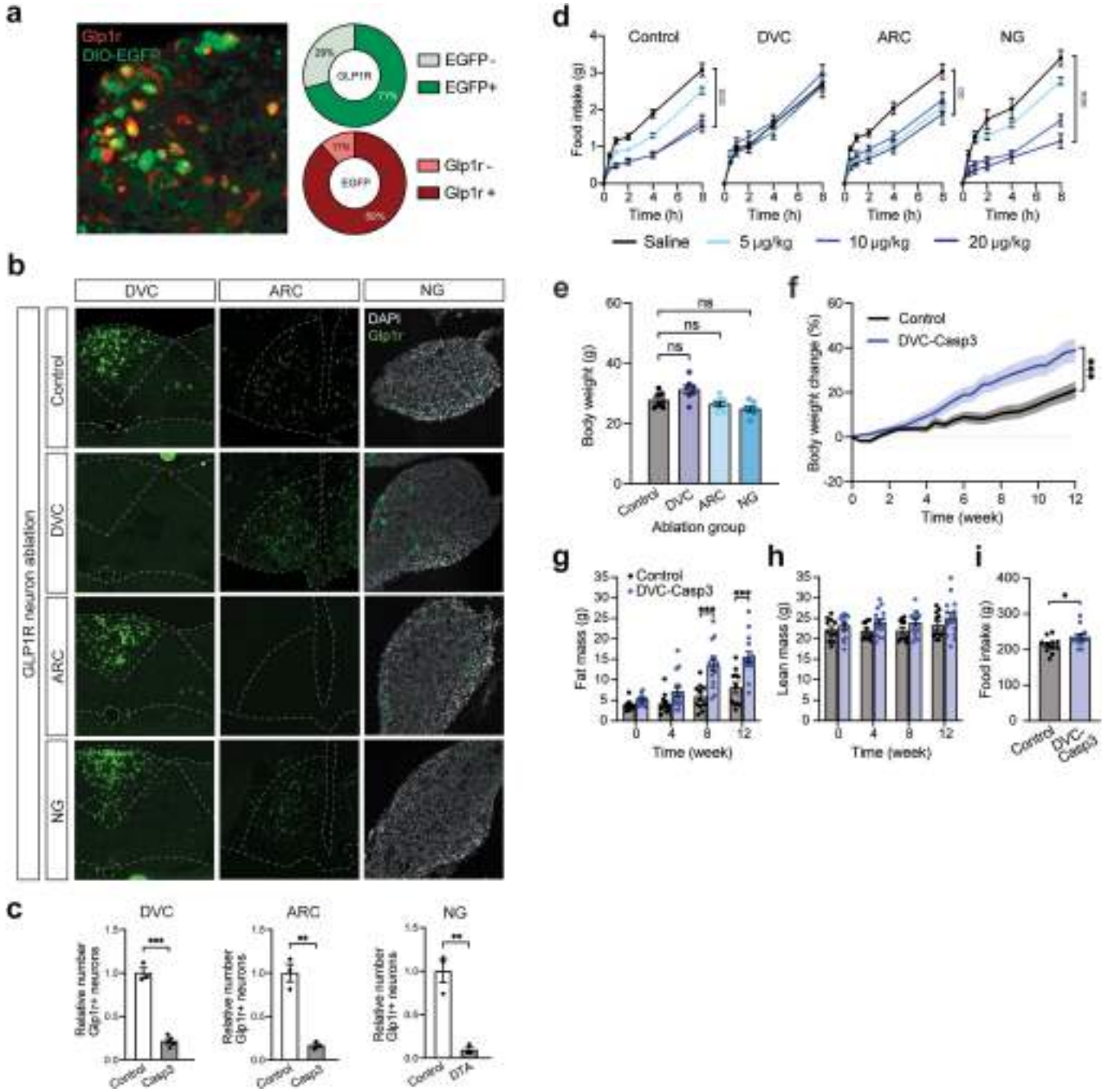

Extended Data Fig. 1 | DVC^{GLP1R} neurons are required for the food intake suppression and weight loss effects of GLP1-based obesity drugs. **a**, Representative image and quantification of viral expression (EGFP) in Glp1r-expessing neurons of *Glp1r-ires-Cre* mice (RNA *in situ* hybridization). **b**, Representative images of Glp1r expression (RNA *in situ* hybridization) in the DVC, ARC, and NG of control mice or mice with GLP1R neuron ablation in each region. **c**, Quantification of Caspase3- or DTA-mediated neural ablation: relative number (to controls) of GLP1R+ neurons in DVC (left), ARC (middle), and NG (right) of mice with viral injection into DVC, ARC, or NG, respectively (n = 3-5 mice/group, two-sided unpaired t-tests, all ps < 0.01). **d**, Food intake following IP injection of saline or exendin-4 in fasted control or GLP1R-ablated mice (n = 8-14 mice/group, two-way repeated measures ANOVAs, all ps < 0.01 except DVC where p=ns). **e**, Body weight at 8 weeks post-surgery in control, DVC, ARC, and NG GLP1R neuron ablation groups (n = 7-8 mice/group, one-way ANOVA, p=ns). **f**, Percent body weight change during the onset of diet-induced obesity in high-fat diet-fed control (EGFP) or DVC^{GLP1R} neuron-ablated mice receiving semaglutide (n = 11-15 mice/group, two-way repeated measures ANOVA, control versus DVC-Casp3, p < 0.001). **g**–**i**, Fat mass (**g**, n = 11-15 mice/group, two-way ANOVA, Control versus DVC-Casp at 8 and 12 weeks: p < 0.001), lean mass (**h**, n = 11-15/group, two-way ANOVA, all ps=ns) and cumulative food intake (**i**, n = 11-13 mice/group, two-sided unpaired t-test, p < 0.05) in high-fat diet-fed control or DVC GLP1R-ablated mice over 12 weeks of biweekly SQ semaglutide. Values are mean ± S.E.M. ¤¤p < 0.01, ¤¤¤p < 0.001 drug x time interaction; *p < 0.05, **p < 0.01, ***p < 0.001 *post hoc* comparisons. See Supplementary Table 1 for statistical details.

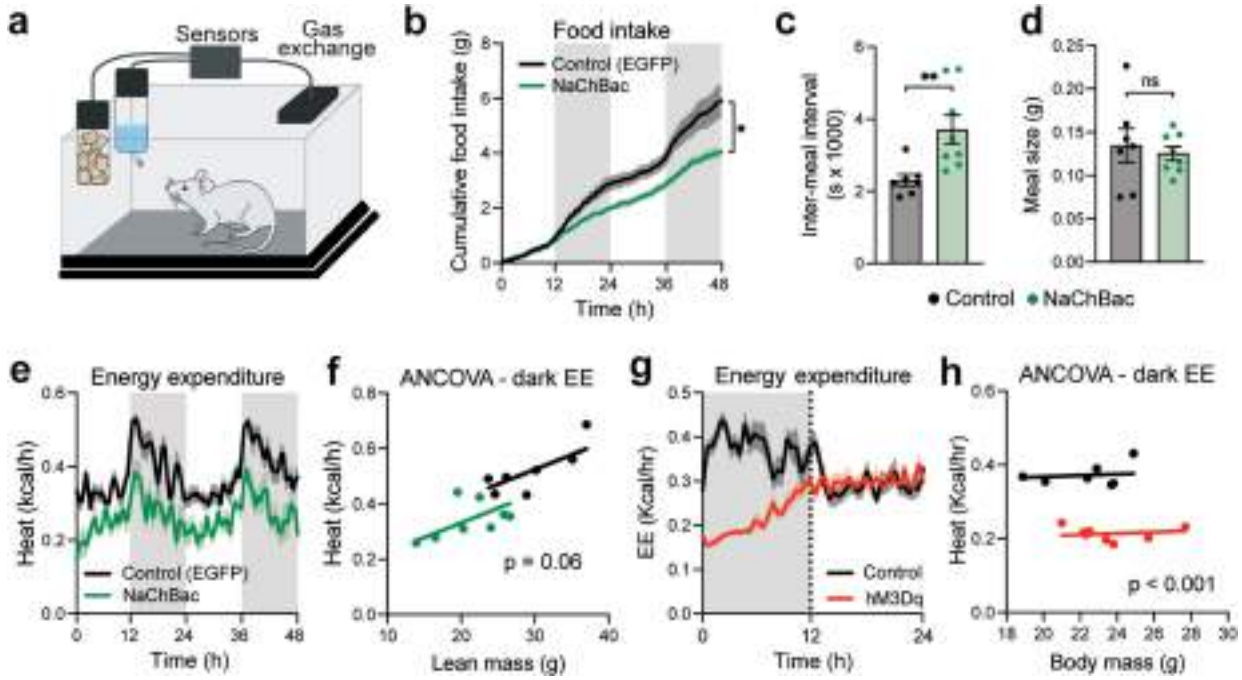

Extended Data Fig. 2 | DVC^{GLP1R} neuron activation suppresses food intake and energy expenditure. a, Schematic for continuous food intake and energy expenditure measurements using mouse metabolic chambers. **b**, Cumulative food intake in high-fat diet-fed control mice or mice with chronic NaChBac-mediated DVC^{GLP1R} neuron activation (n = 7-8 mice/group, two-way repeated measures ANOVA, control versus NaChBac: $p < 0.001$). Shaded areas represent dark periods. **c**, Average inter-meal interval of high-fat diet-fed control mice or mice with chronic NaChBac-mediated DVC^{GLP1R} neuron activation (n = 7-8 mice/group, two-sided unpaired t-test, control versus NaChBac: $p < 0.01$). **d**, Average meal size in high-fat diet-fed control mice or mice with chronic NaChBac-mediated DVC^{GLP1R} neuron activation (n = 7-8 mice/group, two-sided unpaired t-test, control vs. NaChBac: p=ns). **e**, Energy expenditure in high-fat diet-fed control mice or mice with chronic NaChBac-mediated DVC^{GLP1R} neuron activation (n = 7-8 mice/group). Shaded area represents dark period. **f**, Dark period energy expenditure normalized to lean mass by ANCOVA in high-fat diet-fed control mice or mice with chronic NaChBac-mediated DVC^{GLP1R} neuron activation (n = 7-8 mice/group, ANCOVA, $p = 0.06$). **g**, Energy expenditure in fasted chow-fed control mice or mice with chemogenetic DVC^{GLP1R} neuron activation (n = 8 mice/group). Shaded area represents dark period. **h**, Dark period energy expenditure normalized to body mass by ANCOVA in chow-fed control mice or mice with chemogenetic DVC^{GLP1R} neuron activation (n = 8 mice/group, ANCOVA, $p < 0.001$). Values are mean ± S.E.M. $^*p < 0.05$, $^{**}p < 0.01$, $^{***}p < 0.001$. See Supplementary Table 1 for statistical details.

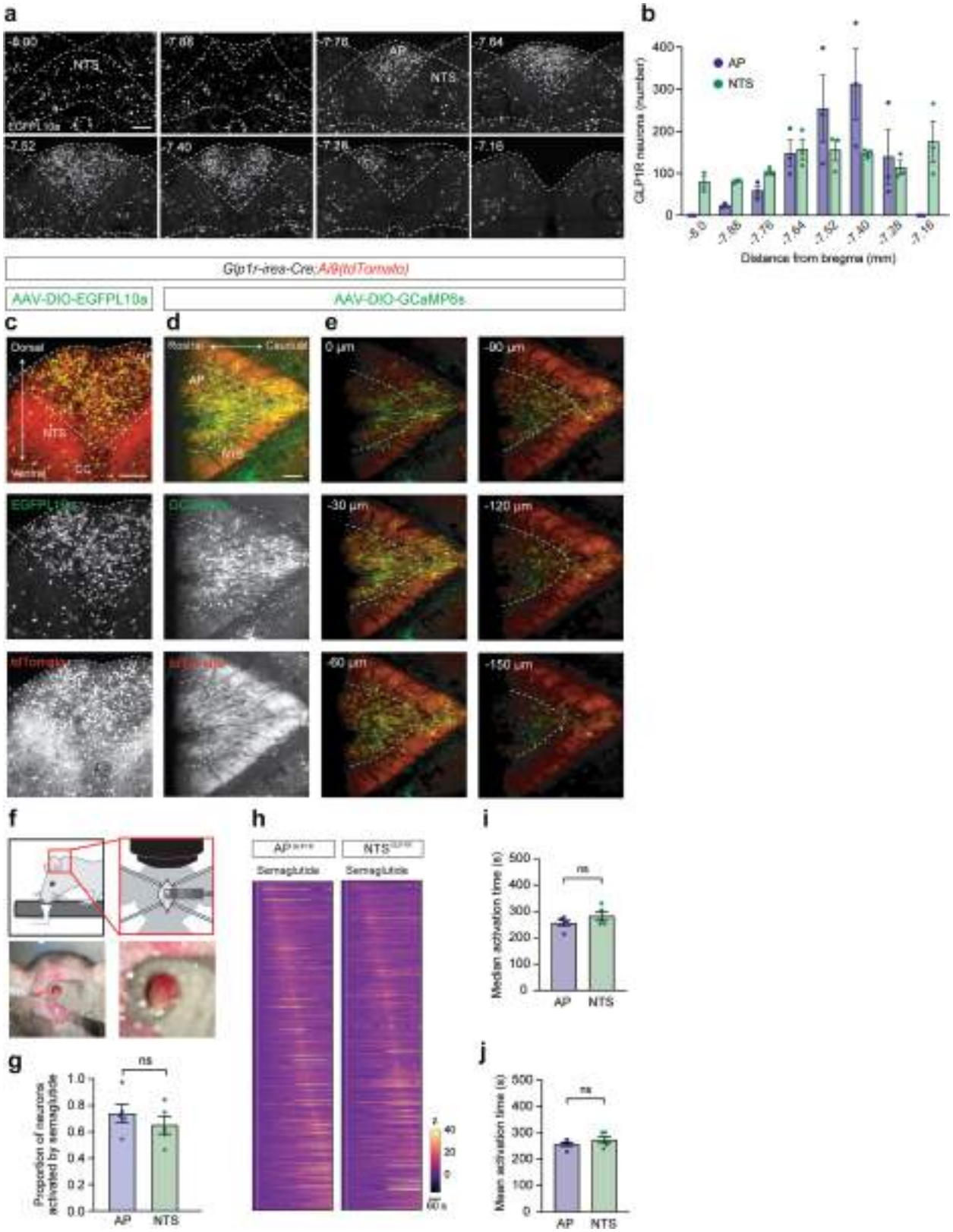

Extended Data Fig. 3 | See next page for caption.

Extended Data Fig. 3 | Imaging AP^{GLP1R} and NTS^{GLP1R} neurons. a, Coronal images of soma-restricted AAV5-EF1a-DIO-EGFPL10a in the DVC of *Glp1r-ires-Cre* mice across the rostral-caudal axis. Scale bar, 100 µm. **b**, Quantification of GLP1R neurons in AP and NTS across the rostral-caudal axis (n = 3 mice/group). **c**, Coronal images of soma-restricted AAV5-EF1a-DIO-EGFPL10a in the DVC of *Glp1r-ires-Cre;Ai9(tdTomato)* mice. Images depict the dense GLP1R projection into the NTS *but not* into the AP. Scale bar, 100 µm. **d**, Maximum projection two-photon images (transverse plane) of the DVC from *Glp1r-ires-Cre;Ai9(tdTomato)* mice injected with Cre-dependent GCaMP6s depicting the red halo of GLP1R projections into the NTS, part of the strategy to draw boundaries between AP and NTS (see Methods for additional details). Scale bar, 100 µm. **e**, Two-photon images of the DVC from *Glp1r-ires-Cre;Ai9(tdTomato)* mice injected with Cre-dependent GCaMP6s across the z-axis. AP and NTS neurons are visible on all imaging planes because of the angle of the medulla for imaging (see Methods for additional details). **f**, Top, schematic for simultaneous in vivo two-photon imaging of AP^{GLP1R} and NTS^{GLP1R} neurons in mice. Bottom, images of surgical prep and cranial window for in vivo two-photon imaging of calcium dynamics in AP^{GLP1R} and NTS^{GLP1R} neurons. **g**, Proportion of AP^{GLP1R} and NTS^{GLP1R} neurons activated by semaglutide (n = 5 mice, two-sided paired t-test, p=ns). **h**, Heat maps depicting z-scored responses of semaglutide-activated AP^{GLP1R} (n = 678 neurons, 5 mice) and NTS^{GLP1R} (n = 388 neurons, 5 mice) neurons sorted by activation time. **i**, Median time to semaglutide-induced activation in AP^{GLP1R} and NTS^{GLP1R} neurons depicted in **h** (n = 5 mice, two-sided unpaired t-test, p=ns). **j**, Mean time to semaglutide-induced activation in AP^{GLP1R} and NTS^{GLP1R} neurons depicted in **h** (n = 5 mice, two-sided unpaired t-test, p=ns). Values are mean ± S.E.M. See Supplementary Table 1 for statistical details.

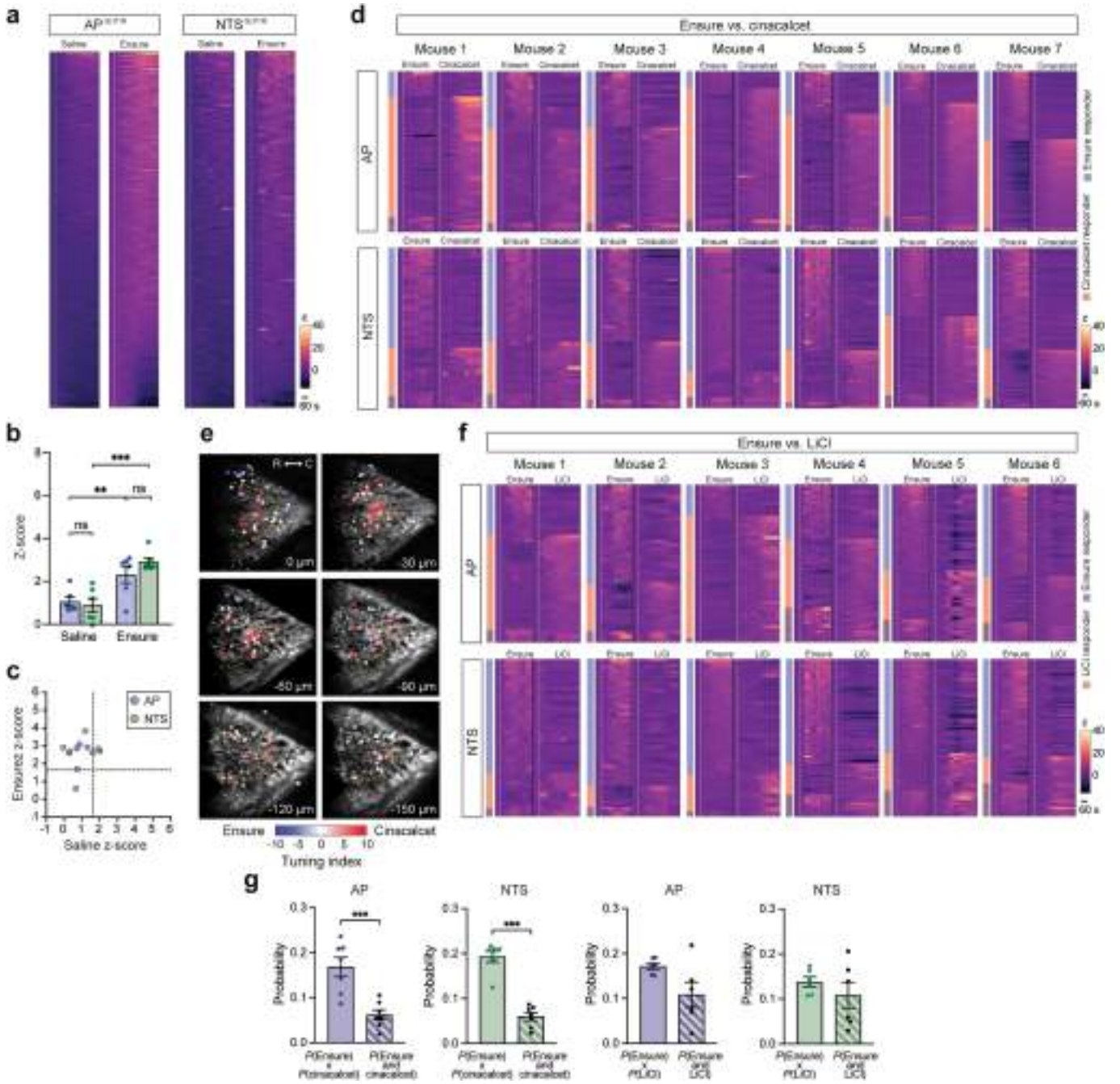

Extended Data Fig. 4 | In vivo responses of AP^{GLP1R} and NTS^{GLP1R} neurons to nutritive and aversive stimuli. a, Heat maps depicting z-scored responses of AP^{GLP1R} neurons (n = 375 neurons, 5 mice) and NTS^{GLP1R} neurons (n = 266 neurons, 5 mice) to saline or Ensure. Dashed white lines indicate start of stimulus. **b**, Average z-scored activity responses in AP^{GLP1R} neurons (blue) and NTS^{GLP1R} neurons (green) to saline or Ensure administration (n = 6 mice, two-way ANOVA, AP: saline versus Ensure: $p < 0.01$, NTS: saline versus Ensure $p < 0.001$). **c**, Individual data points comparing AP^{GLP1R} (blue) and NTS^{GLP1R} (green) neuron z-scored activity responses to saline and semaglutide. Dotted lines represent threshold for statistically significant neural activation (z = 1.64, see Methods for additional details). **d**, Individual heat maps for each mouse (n = 7) depicting z-scored responses of AP^{GLP1R} and NTS^{GLP1R} neurons to Ensure or cinacalcet. **e**, Representative two-photon images of GCaMP6s across the z axis with neurons colour-coded based on responses to Ensure (most responsive in blue, index = −10) and cinacalcet (most responsive in red, index=10). AP/NTS boundary indicated in yellow. **f**, Individual heat maps for each mouse (n = 6) depicting z-scored responses of AP^{GLP1R} and NTS^{GLP1R} neurons to Ensure or LiCl. **g**, Probability calculations for activation of individual cells by Ensure or aversive stimuli (n = 6-7 mice/group, two-sided paired t-tests, $p < 0.001$). We compare the product of the probabilities of a neuron being activated by either Ensure or aversive stimuli [*P*(Ensure) x P(cinacalcet) or *P*(Ensure) x *P*(LiCl)] to the probability of a neuron being activated by both stimuli [*P*(Ensure and cinacalcet) or *P*(Ensure and LiCl)]. That the probability of a cell being activated by both stimuli is generally lower than the product of individual probabilities suggests a level of specialization of individual cells where most are biased toward nutritive or aversive stimuli, with less overlap than would be expected by chance. Values are mean ± S.E.M. *p < 0.05, **p < 0.01, ***p < 0.001. See Supplementary Table 1 for statistical details.

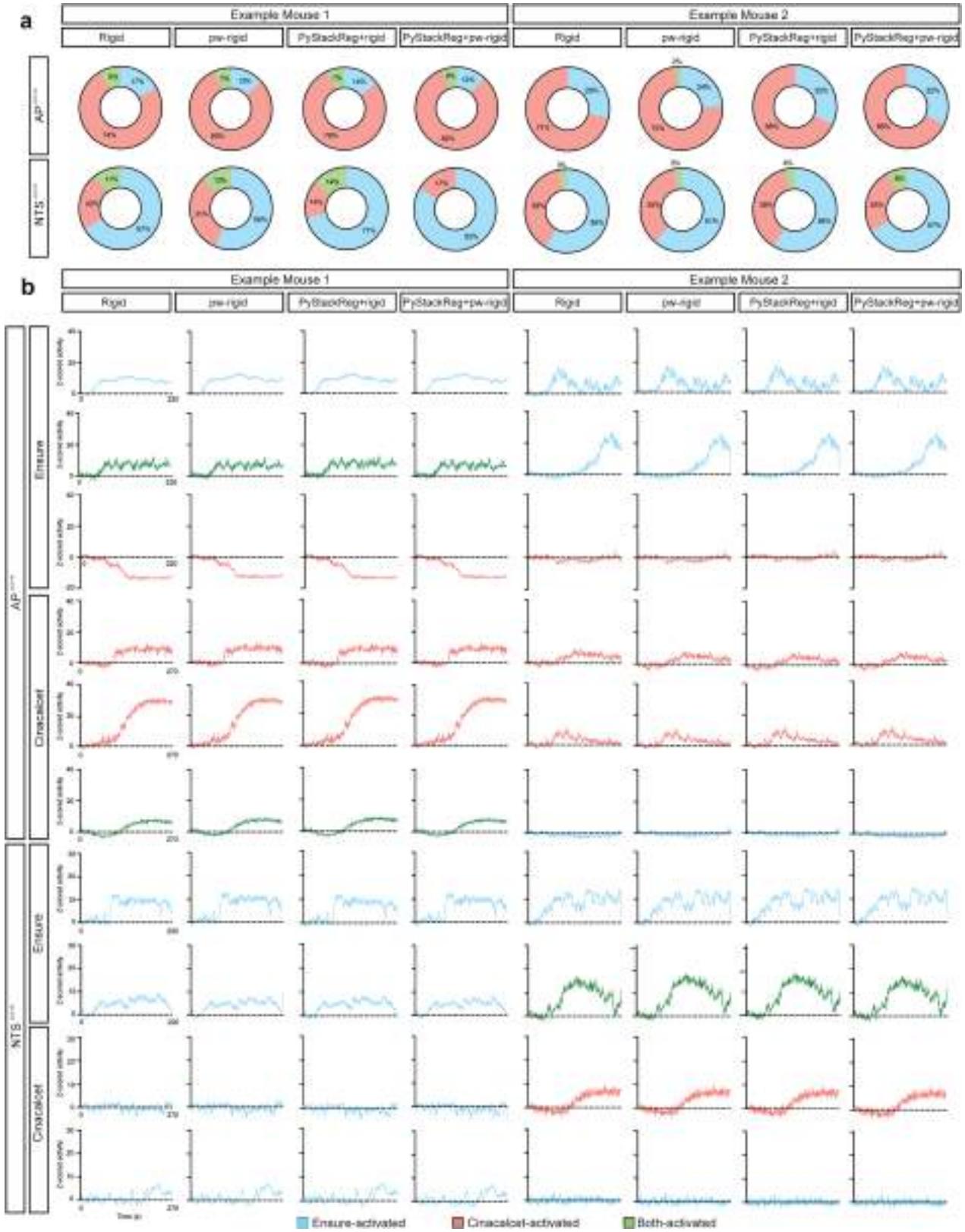

Extended Data Fig. 5 | See next page for caption.

Extended Data Fig. 5 | Comparison of motion correction strategies for extracting calcium dynamics. To determine whether alternate motion correction strategies improved calcium imaging analyses in our setup, we compared rigid-body motion correction ("Rigid") with two other strategies (and the two strategies combined). First, we applied the piecewise rigid function ("pw-rigid") in NoRMCorre to create a grid within each of our images, where each patch of the grid was corrected to better adjust for non-rigid distortions. Second, we applied PyStackReg to realign all frames using an affine transformation. We compared the resulting proportions of activated neurons and individual neuron calcium traces for each method. Although these alternate motion correction strategies did not significantly change our data, we note for readers that some imaging preparations (especially those that have more ROIs around the edges of frames) may require such strategies. **a**, Comparison of proportions of neurons activated by nutritive (Ensure, blue), aversive (cinacalcet, pink), or both (green) stimuli in AP^{GLP1R} and NTS^{GLP1R} neurons across one z-level from each of two example mice chosen at random, after imaging analysis following different motion correction strategies. **b**, Comparison of individual neuron calcium traces in AP^{GLP1R} and NTS^{GLP1R} neurons activated by nutritive (Ensure, blue), aversive (cinacalcet, pink), or both (green) stimuli after imaging analysis following different motion correction strategies. Traces were chosen pseudo-randomly, excluding neurons that were not selected as ROIs in each of the four analyses [these, however, were included in **a**, where we did not exclude any neurons], and accounting for representation of Ensure-activated, cinacalcet-activated, and both-activated neurons where possible.

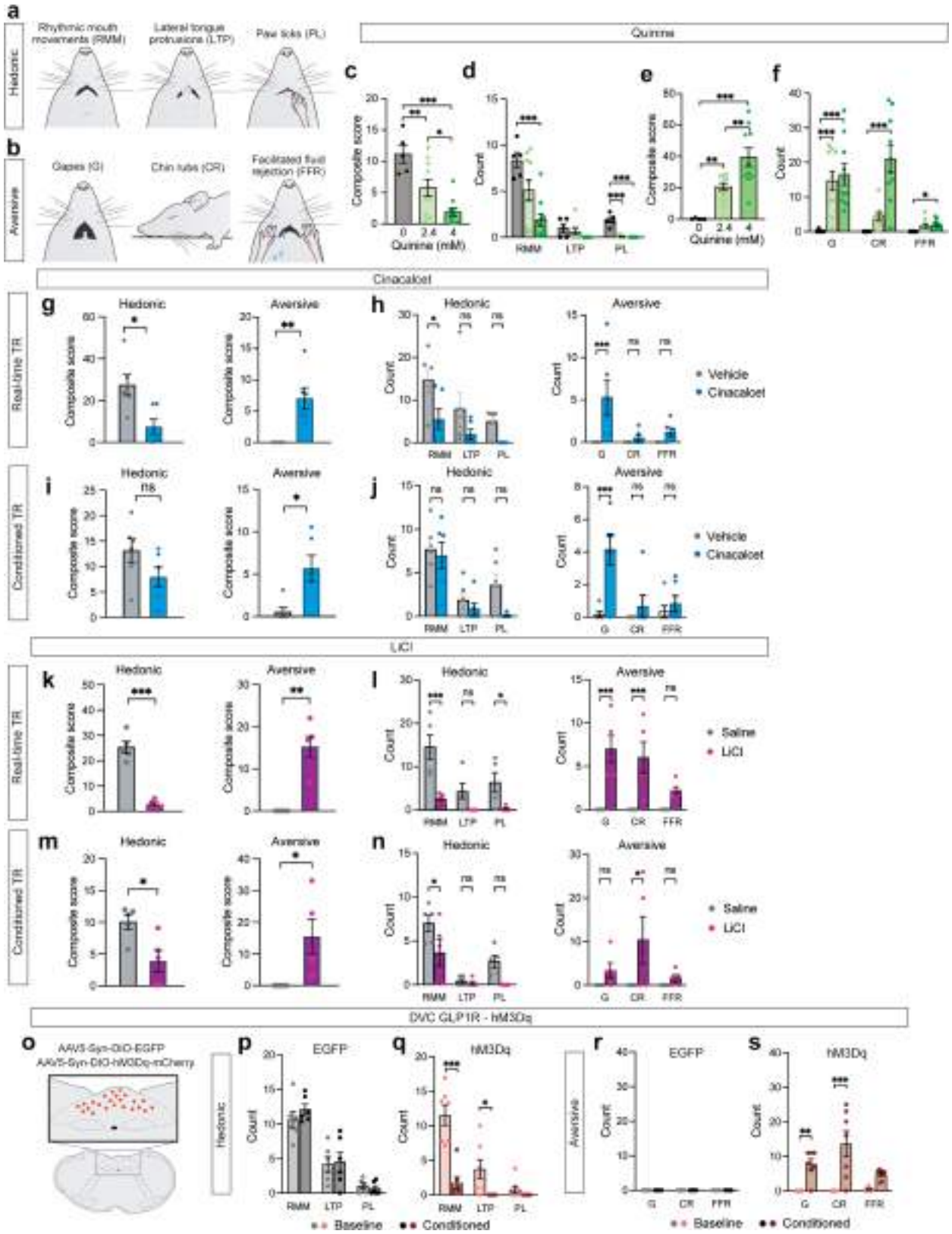

Extended Data Fig. 6 | See next page for caption.

Extended Data Fig. 6 | Real-time and conditioned orofacial taste reactivity in mice. a,**b**, Schematics of stereotyped hedonic (**a**) and aversive (**b**) orofacial responses in mice. Modified from schematics in ref. 22. **c**,**d**, Composite score (**c**, n = 5-10 mice/group, one-way ANOVA, all ps<0.05) and individual behaviours (**d**, n = 5-10 mice/group, two-way ANOVA, all ps<0.001) for hedonic taste reactivity responses to quinine concentrations (0, 2.4, 4 mM). **e**,**f**, Composite score (**e**, n = 5-10 mice/group, one-way ANOVA, all ps<0.01) and individual behaviours (**f**, 5-10 mice/group, two-way ANOVA, all ps<0.05) for aversive taste reactivity responses to quinine concentrations (0, 2.4, 4 mM). **g**,**h**, Composite scores (**g**, n = 6 mice/group, two-sided paired t-tests, ps<0.05) and individual behaviours (**h**, 6 mice/group, two-way ANOVA, RMM: $p < 0.05$, G: $p < 0.001$) for real-time hedonic and aversive taste reactivity responses to a flavour paired with cinacalcet (15 µmol/kg, IP). **i**,**j**, Composite scores (**i**, n = 6 mice/group, two-sided paired t-tests, aversive: $p < 0.05$) and individual behaviours (**j**, 6 mice/group, two-way ANOVA, G: $p < 0.001$) for conditioned hedonic and aversive taste reactivity responses to a flavour paired with cinacalcet (15 µmol/kg, IP). **k**,**l**, Composite scores (**k**, n = 5 mice/group, two-sided paired t-tests, ps<0.01) and individual behaviours (**l**, 6 mice/group, two-way ANOVA, RMM: $p < 0.001$, PL: $p < 0.05$, G: $p < 0.001$, CR: $p < 0.001$) for real-time hedonic and aversive taste reactivity responses to a flavour paired with LiCl (6 mmol/kg, IP). **m**,**n**, Composite scores (m, n = 5 mice/group, two-sided paired t-tests, ps<0.05) and individual behaviours (n = 6 mice/group, two-way ANOVA, RMM: $p < 0.05$, G: $p < 0.001$, CR: $p < 0.05$) for conditioned hedonic and aversive taste reactivity responses to a flavour paired with LiCl (6 mmol/kg, IP). **o**, Schematic for chemogenetic stimulation of DVC^{GLP1R} neurons. **p**,**q**, Individual hedonic taste reactivity behaviours at baseline and after conditioning in control (**p**, n = 6 mice/group, two-way ANOVA, all ps=ns) and experimental (**q**, n = 7 mice/group, two-way ANOVA, RMM: $p < 0.001$, LTP: $p < 0.05$) mice. **r**,**s**, Individual aversive taste reactivity behaviours at baseline and after conditioning in control (**r**, n = 6 mice/group, two-way ANOVA, all ps=ns) and experimental (**s**, n = 7 mice/group, two-way ANOVA, G: $p < 0.01$, CR: $p < 0.001$) mice. Values are mean ± S.E.M. *$p < 0.05$, **$p < 0.01$, ***$p < 0.001$. See Supplementary Table 1 for statistical details.

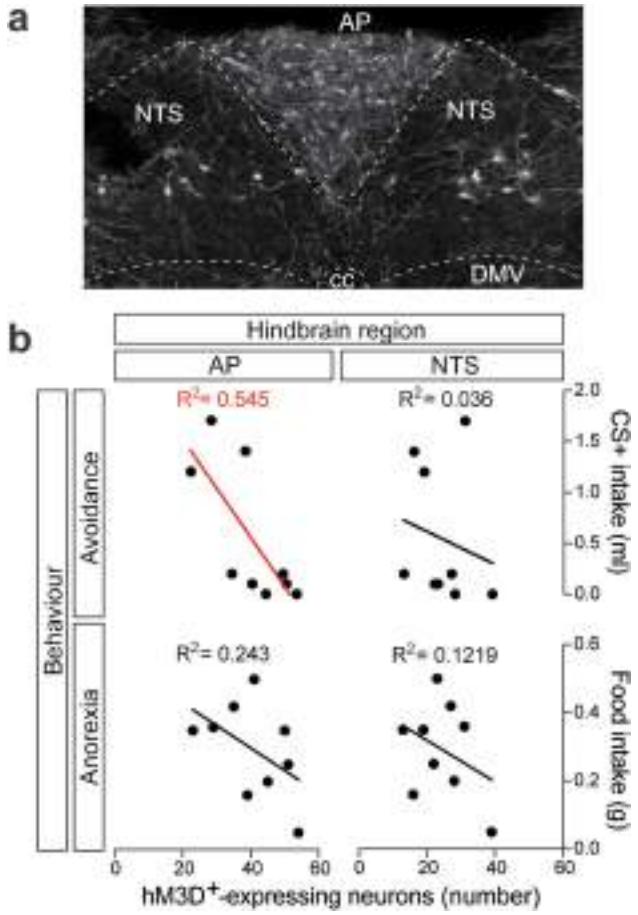

Extended Data Fig. 7 | Number of AP^{GLP1R}, but not NTS^{GLP1R}, neurons expressing chemogenetic receptors correlates with avoidance behaviour. **a**, Representative image of hM3Dq expression in the DVC (AP and NTS). **b**, Correlation between the number of hM3Dq-expressing neurons (x-axis) and behaviour [y-axis; avoidance (CS+ intake in CFA assay) or anorexia (food intake) elicited by DVC^{GLP1R} neuron stimulation] in the AP (left graphs) or NTS (right graphs) (n = 9 mice, Pearson correlation, $p < 0.05$ for AP/avoidance, other ps=ns). Red colour indicates statistical significance. See Supplementary Table 1 for statistical details.

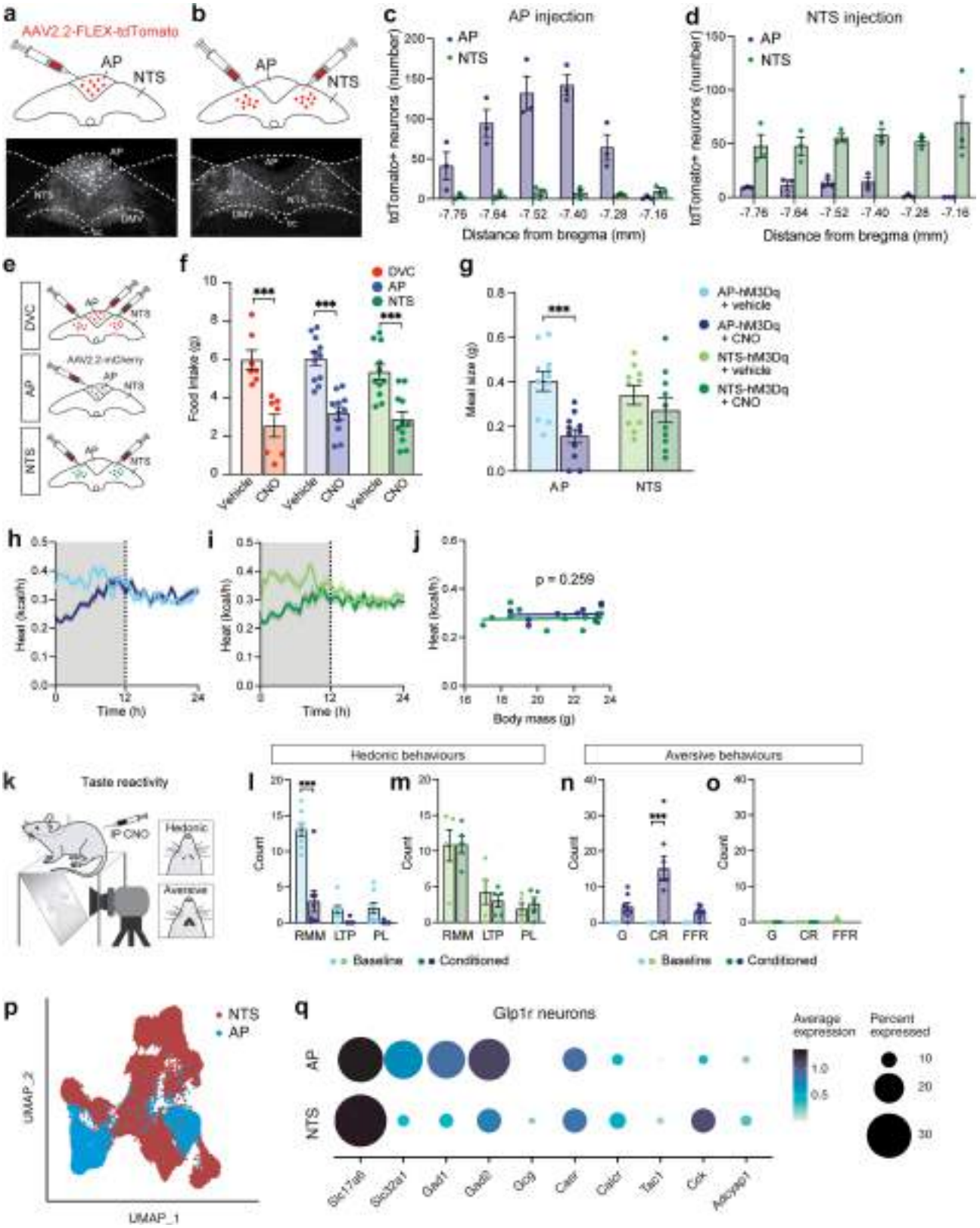

Extended Data Fig. 8 | See next page for caption.

Extended Data Fig. 8 | AP^{GLP1R} and NTS^{GLP1R} neurons are largely unique populations of hindbrain neurons with dissociable behavioural effects. a,**b**, Schematic and representative images of viral (AAV2.2-FLEX-tdTomato) separation of AP (**a**) and NTS (**b**) using 20 nl intracranial injections. **c**, Quantification of tdTomato-expressing GLP1R neurons in AP and NTS after viral injection into AP (n = 3 mice). **d**, Quantification of tdTomato-expressing GLP1R neurons in AP and NTS after viral injection into NTS (n = 3 mice). **e**, Strategy for viral injections to directly compare behavioural results of activation of DVC^{GLP1R}, AP^{GLP1R}, and NTS^{GLP1R} neurons: we used the same viral serotype and injection protocol to activate neurons in each of these regions. **f**, 12-h food intake in mice following activation of DVC^{GLP1R}, AP^{GLP1R}, and NTS^{GLP1R} neurons (n = 7-11 mice/group, two-way ANOVA, all ps<0.001). **g**, Meal size in fasted mice following chemogenetic activation of AP^{GLP1R} or NTS^{GLP1R} neurons (n = 10-11 mice/group, two-way ANOVA, AP^{GLP1R}-hM3Dq vehicle versus CNO: $p < 0.001$, NTS^{GLP1R}-hM3Dq vehicle versus CNO: p=ns). **h**,**i**, Energy expenditure in fasted mice with chemogenetic AP^{GLP1R} (**h**) or NTS^{GLP1R} (**i**) neuron activation (n = 11 mice/group). Shaded area represents dark period. **j**, Dark period energy expenditure normalized to body mass by ANCOVA in mice with chemogenetic AP^{GLP1R} (blue) or NTS^{GLP1R} (green) neuron activation (n = 11 mice/group, ANCOVA, p=ns). **k**, Schematic describing protocol for taste reactivity experiments. **l**,**m**, Individual hedonic taste reactivity behaviours at baseline and after conditioning with chemogenetic AP^{GLP1R} (**l**, n = 8 mice, two-way ANOVA, RMM baseline versus conditioned $p < 0.001$) or NTS^{GLP1R} (**m**, n = 5 mice, two-way ANOVA, all ps=ns) neuron activation. **n**,**o**, Individual aversive taste reactivity behaviours at baseline and after conditioning with chemogenetic AP^{GLP1R} (**n**, n = 8 mice, two-way ANOVA, CR baseline versus conditioned: $p < 0.001$) or NTS^{GLP1R} (**o**, n = 5 mice, two-way ANOVA, all ps=ns) neuron activation. **p**, Uniform manifold approximation and projection (UMAP) plot showing AP and NTS neuron subtypes. Analysis was made after combining data sets from ref. 13, ref. 16, and ref. 17, which all contained cells from both the AP and NTS. **q**, Dot plots indicating normalized expression of genes in *Glp1r*+ cells of the AP and NTS. Values are mean ± S.E.M. *$p < 0.05$, **$p < 0.01$, ***$p < 0.001$. See Supplementary Table 1 for statistical details.

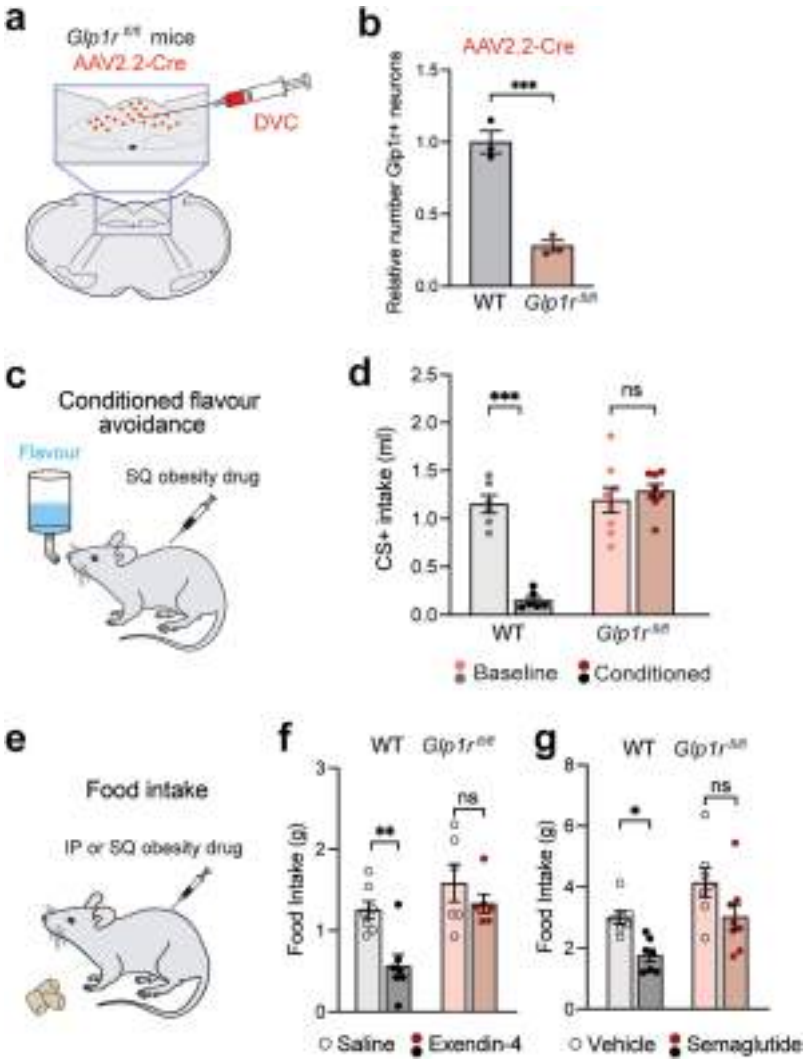

Extended Data Fig. 9 | Deletion of GLP1R in DVC attenuates anorexia and aversion by obesity drugs. a, Schematic for deletion of GLP1R in DVC neurons using *Glp1r*$^{fl/fl}$ mice and injection of AAV2.2-Cre. **b**, Quantification of efficacy of GLP1R deletion: relative number of *Glp1r*+ neurons in the DVC in WT and *Glp1r*$^{fl/fl}$ mice after DVC injection of AAV2.2-Cre (n = 3 mice/group, two-sided unpaired t-test, $p < 0.001$). **c**, Mice underwent a conditioned flavour avoidance assay to semaglutide. **d**, Intake of flavour paired with semaglutide (CS+) in control (WT) or DVC GLP1R-deleted (*Glp1r*$^{fl/fl}$) mice before (baseline) and after conditioning (n = 6-8 mice/group, two-way ANOVA, WT baseline versus conditioned: $p < 0.001$, *Glp1r*$^{fl/fl}$ baseline vs. conditioned: p=ns). **e**, Food intake (4 h) was measured in response to exendin-4 or semaglutide. For exendin-4 studies, food was returned immediately after injection. For semaglutide studies, food was returned 4 h post-injection. **f**, Food intake in response to exendin-4 in WT and *Glp1r*$^{fl/fl}$ mice (**e**, n = 6-7 mice/group, two-way ANOVA, WT: $p < 0.01$, *Glp1r*$^{fl/fl}$: p=ns). **g**, Food intake in response to semaglutide in WT and *Glp1r*$^{fl/fl}$ mice (**e**, n = 7-8 mice/group, two-way ANOVA, WT: $p < 0.05$, *Glp1r*$^{fl/fl}$: p=ns). Values are mean ± S.E.M. *$p < 0.05$, **$p < 0.01$, ***$p < 0.001$. See Supplementary Table 1 for statistical details.

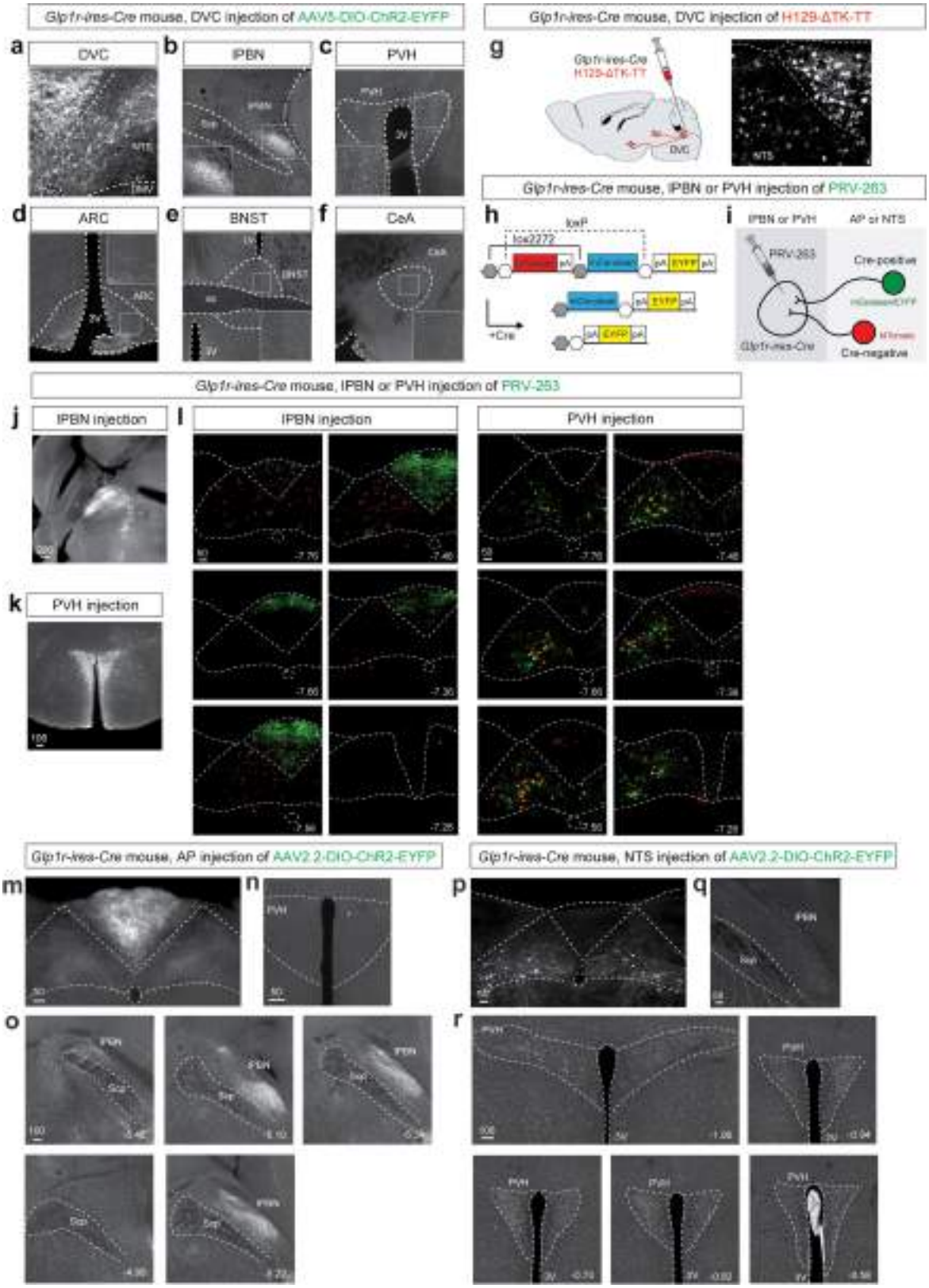

Extended Data Fig. 10 | See next page for caption.

Extended Data Fig. 10 | Representative images and injection verifications for neural tracing experiments. a, Representative image of viral expression of AAV5-DIO-ChR2-EYFP at the injection site (DVC: AP and NTS) of *Glp1r-ires-Cre* mice (n = 3 mice). cc, central canal; DMV, dorsal motor nucleus of the vagus. **b**–**f**, Representative images of DVC^{GLP1R} axons in brain regions involved in feeding behaviour: lPBN (**b**), PVH (**c**), ARC (**d**), BNST (**e**), CeA (**f**). Boxes indicate zoomed in regions. 3 V, third ventricle; ac, anterior commissure; BNST, bed nucleus of the stria terminalis; CeA, central amygdala; LV, lateral ventricle; Scp, superior cerebellar peduncle. **g**, Left, Cre-dependent H129-ΔTK-TT was injected into the DVC of *Glp1r-ires-Cre* mice (n = 3). Right, representative image of starter cells for anterograde H129-ΔTK-TT-mediated tracing from DVC^{GLP1R} neurons. **h**, Schematic of mechanism for fluorophore expression using PRV-263. **i**, *Glp1r-ires-Cre* mice (n = 3 mice/group) were injected in the lPBN or PVH with PRV-263 and DVC brain sections were imaged for retrogradely-transported Cre-positive (GLP1R+, mCerulean/EYFP, green) and Cre-negative (GLP1R−, tdTomato, red) neurons in the AP and NTS. **j**, Representative image of lPBN injection site. Scale bar, 200 µm. **k**, Representative image of PVH injection site. Scale bar, 100 µm. **l**, Representative images of PRV-263 in Cre-positive (GLP1R+, mCerulean/EYFP, green) and Cre-negative (GLP1R-, tdTomato, red) neurons of the AP and NTS after viral injection in the lPBN (left) or PVH (right). Distances indicate mm from bregma. Scale bar, 50 µm. **m**, Representative image of injection site in AP after injection of Cre-dependent AAV2.2-DIO-ChR2-EYFP in AP^{GLP1R} neurons in *Glp1r-ires-Cre* mice (n = 3 mice). Scale bar, 50 µm. **n**, Representative image of PVH in mouse with EYFP injection in AP^{GLP1R} neurons. Scale bar, 50 µm. **o**, Representative images of PBN projections across the rostral-caudal axis, distances indicate mm from bregma. **p**, Representative image of injection site in NTS after injection of Cre-dependent AAV2.2-DIO-ChR2-EYFP in NTS^{GLP1R} neurons in *Glp1r-ires-Cre* mice (n = 3 mice). Scale bar, 50 µm. **q**, Representative image of lPBN in mouse with EYFP injection in NTS^{GLP1R} neurons. Scale bar, 50 µm. **r**, Representative images of PVH projections across the rostral-caudal axis, distances indicate mm from bregma. Scale bar, 100 µm.

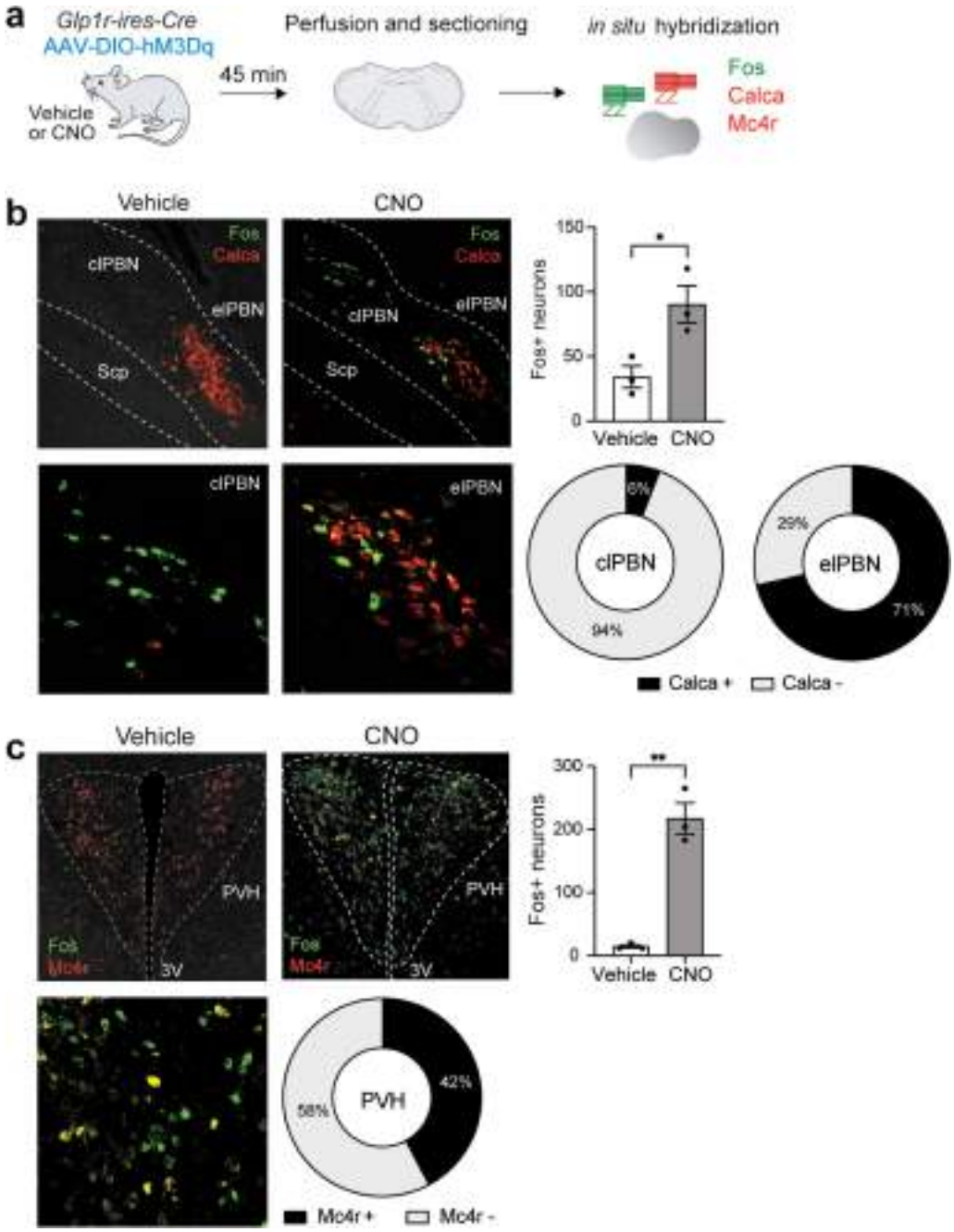

Extended Data Fig. 11 | Neural activation in the lPBN and PVH with DVC^{GLP1R} neuron stimulation. a, Schematic for RNA in situ hybridization for Fos and CGRP (Calca) in lPBN or Fos and Mc4r in PVH after chemogenetic stimulation of DVC^{GLP1R} neurons. **b**, Representative images (left) and quantification (right) of colocalization of Fos and Calca in the lPBN after control (vehicle) or chemogenetic (CNO) stimulation (n = 3 mice/group, two-sided unpaired t-test, $p < 0.05$). elPBN, external lateral PBN; clPBN, central lateral PBN. **c**, Representative images (left) and quantification (right) of Fos and Mc4r in the PVH after control (vehicle) or chemogenetic (CNO) stimulation (n = 3 mice/group, two-sided unpaired t-test, $p < 0.01$). Values are mean ± S.E.M. *$p < 0.05$, **$p < 0.01$.

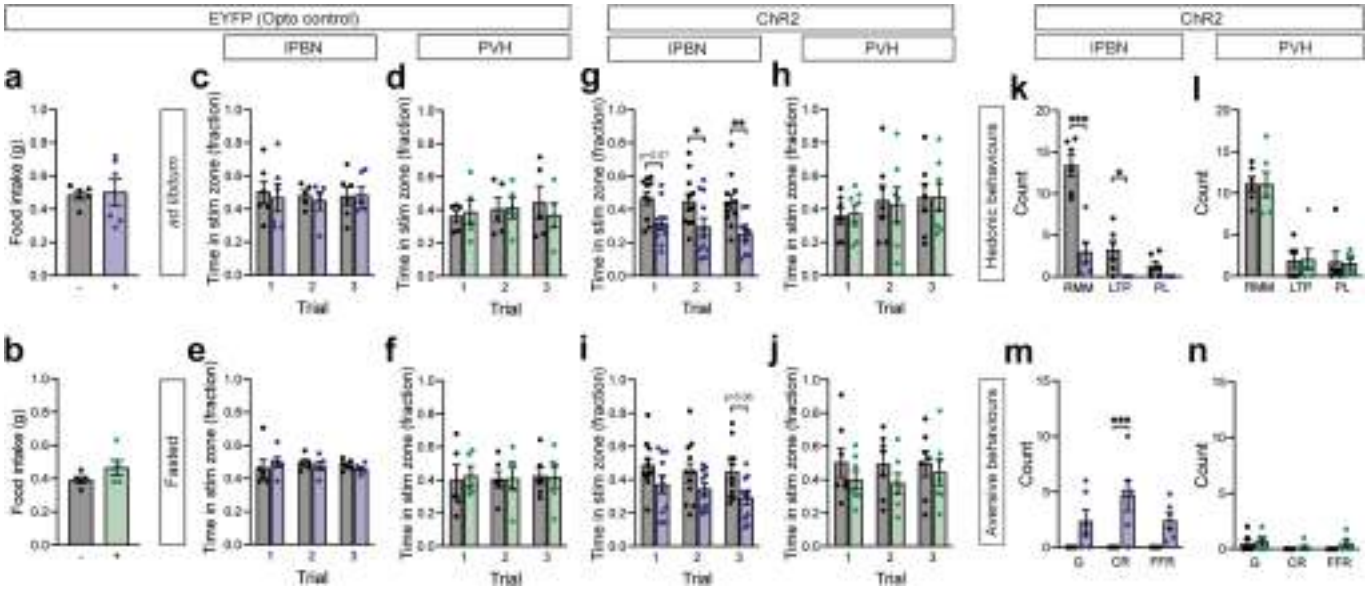

Extended Data Fig. 12 | Behavioural effects of AP^{GLP1R}→lPBN and NTS^{GLP1R}→PVH neuron optogenetic activation. a,**b**, Food intake (1 h) in control mice expressing EYFP in AP^{GLP1R}→lPBN (**a**, n = 6 mice, paired t-test, p=ns) and NTS^{GLP1R}→PVH (**b**, n = 5 mice, two-sided paired t-test, p=ns) neurons. (Grey bars (–), no stimulation; coloured bars (+), stimulation). **c**,**d**, Time spent in stimulation zone during real-time place avoidance assay in *ad libitum*-fed control mice expressing EYFP in AP^{GLP1R}→lPBN (**c**, n = 5-6 mice/group, two-way ANOVA, all ps=ns) or NTS^{GLP1R}→PVH (**d**, n = 5 mice, two-way ANOVA, all ps=ns) neurons. **e**,**f**, Time spent in stimulation zone during real-time place avoidance assay in fasted control mice expressing EYFP in AP^{GLP1R}→lPBN (**e**, n = 5-6 mice/group, two-way ANOVA, all ps=ns) or NTS^{GLP1R}→PVH (**f**, n = 5-6 mice/group, two-way ANOVA, all ps=ns). **g**,**h**, Time spent in stimulation zone during real-time place avoidance assay in *ad libitum*-fed mice expressing ChR2 in AP^{GLP1R}→lPBN (**g**, n = 10-11 mice/group, two-way ANOVA, Trials 2&3 no stim versus stim: ps<0.05) or NTS^{GLP1R}→PVH (**h**, n = 7 mice, two-way ANOVA, all ps=ns). **i**,**j**, Time spent in stimulation zone during real-time place avoidance assay in fasted mice expressing ChR2 in AP^{GLP1R}→lPBN (**i**, n = 11 mice, two-way ANOVA, all ps=ns) or NTS^{GLP1R}→PVH (**j**, n = 7 mice, two-way ANOVA, all ps=ns) neurons. **k**,**l**, Individual hedonic taste reactivity behaviours at baseline (pre-stimulation) and during optogenetic stimulation of AP^{GLP1R}→lPBN (**k**, n = 6 mice, two-way ANOVA, RMM and LTP no stim versus stim: ps<0.05) or NTS^{GLP1R}→PVH (**l**, n = 6 mice, two-way ANOVA, all ps=ns) neurons. **m**,**n**, Individual aversive taste reactivity behaviours at baseline (pre-stimulation) and during optogenetic stimulation of AP^{GLP1R}→lPBN (**m**, n = 6 mice, two-way ANOVA, CR no stim versus stim: $p < 0.001$) or NTS^{GLP1R}→PVH (**n**, n = 6 mice, two-way ANOVA, all ps=ns) neurons. Grey bars, no stimulation; coloured bars, optogenetic stimulation. Values are mean ± S.E.M. *$p < 0.05$, **$p < 0.01$, ***$p < 0.001$. See Supplementary Table 1 for statistical details.

nature portfolio

Corresponding author(s): Amber L Alhadeff

Last updated by author(s): May 16, 2024

Reporting Summary

Nature Portfolio wishes to improve the reproducibility of the work that we publish. This form provides structure for consistency and transparency in reporting. For further information on Nature Portfolio policies, see our Editorial Policies and the Editorial Policy Checklist.

Statistics

For all statistical analyses, confirm that the following items are present in the figure legend, table legend, main text, or Methods section.

n/a	Confirmed	
☐	☒	The exact sample size (*n*) for each experimental group/condition, given as a discrete number and unit of measurement
☐	☒	A statement on whether measurements were taken from distinct samples or whether the same sample was measured repeatedly
☐	☒	The statistical test(s) used AND whether they are one- or two-sided *Only common tests should be described solely by name; describe more complex techniques in the Methods section.*
☐	☒	A description of all covariates tested
☐	☒	A description of any assumptions or corrections, such as tests of normality and adjustment for multiple comparisons
☐	☒	A full description of the statistical parameters including central tendency (e.g. means) or other basic estimates (e.g. regression coefficient) AND variation (e.g. standard deviation) or associated estimates of uncertainty (e.g. confidence intervals)
☐	☒	For null hypothesis testing, the test statistic (e.g. *F*, *t*, *r*) with confidence intervals, effect sizes, degrees of freedom and *P* value noted *Give P values as exact values whenever suitable.*
☒	☐	For Bayesian analysis, information on the choice of priors and Markov chain Monte Carlo settings
☒	☐	For hierarchical and complex designs, identification of the appropriate level for tests and full reporting of outcomes
☐	☒	Estimates of effect sizes (e.g. Cohen's *d*, Pearson's *r*), indicating how they were calculated

Our web collection on statistics for biologists contains articles on many of the points above.

Software and code

Policy information about availability of computer code

Data collection	Two-photon images were acquired using Prairie View (Bruker, v5.7) software. Continuous food intake and energy expenditure measurements were collected using PhenoMaster 's (TSE, v5.0.6) or Promethion's (Sable, v23.0.01) custom software. Orofacial taste reactivity videos were analyzed using iMovie (v10.2.2). Real-time place avoidance data were acquired with EthoVision XT 16 (Noldus) software.
Data analysis	Python (v3.11.6), Prism (v.10.2.2), and Seurat (v.4.3.0) in R (v.4.3.0) software were used for data and statistical analyses. Python packages included CaImAn (v1.9.16), NoRMCorre (v0.1.1), Cellpose (v2.0.5), PyStackReg (v0.2.7). ggplot2 (v3.5.0) was used for transcriptomics analyses. Custom codes are available at https://github.com/alhadefflab/2p_imaging_analysis.

For manuscripts utilizing custom algorithms or software that are central to the research but not yet described in published literature, software must be made available to editors and reviewers. We strongly encourage code deposition in a community repository (e.g. GitHub). See the Nature Portfolio guidelines for submitting code & software for further information.

Data

Policy information about availability of data

All manuscripts must include a data availability statement. This statement should provide the following information, where applicable:

- Accession codes, unique identifiers, or web links for publicly available datasets
- A description of any restrictions on data availability
- For clinical datasets or third party data, please ensure that the statement adheres to our policy

Source data are provided with this paper.

Human research participants

Policy information about studies involving human research participants and Sex and Gender in Research.

Reporting on sex and gender	N/A
Population characteristics	N/A
Recruitment	N/A
Ethics oversight	N/A

Note that full information on the approval of the study protocol must also be provided in the manuscript.

Field-specific reporting

Please select the one below that is the best fit for your research. If you are not sure, read the appropriate sections before making your selection.

☒ Life sciences ☐ Behavioural & social sciences ☐ Ecological, evolutionary & environmental sciences

For a reference copy of the document with all sections, see nature.com/documents/nr-reporting-summary-flat.pdf

Life sciences study design

All studies must disclose on these points even when the disclosure is negative.

Sample size	Power analyses were run [beta = 0.2 (80% power), alpha =0.05) with effect sizes based on pilot studies (n=3-6) to ensure that sample sizes (number of mice for behavioural studies, number of neurons for physiological/anatomical studies) were sufficient to determine significant differences between groups. Based on these results, we repeated experiments in an additional cohort (or cohorts) of mice. For neural imaging we used 5-7 mice, and for and anatomical experiments (comparing proportions of neurons), we analyzed 3 brain sections per mouse from at least 3 mice per group, which are standard sample sizes for imaging and anatomical studies in the neuroscience field.
Data exclusions	There were no exclusions from the data except for the following: For food intake measurements, mice with significant spillage were excluded from analysis (n=3 from DVC NaChBac studies, n=5 from Casp3/DTA/control ablation studies, and n=3 from GLP1R deletion studies). For neural ablation experiments (across several cohorts of 5 experimental groups of mice), n=4 mice were excluded because of unexpected illness and euthanasia during experimentation. For meal pattern analyses, mice with no food intake were excluded from inter-meal interval analyses (n=2 mice in APGLP1R vs. NTSGLP1R chemogenetic stimulation experiments). Across all taste reactivity experiments, n=1 mouse was excluded for a strong aversive response at baseline. For real-time place avoidance studies, n=3 data points were excluded due to mice escaping the apparatus. Where appropriate, viral expression was verified post-mortem; any mouse that did not express virus or expressed virus outside of the target region was excluded from analyses.
Replication	All behavioural experiments were performed in at least two cohorts, and data were combined and analyzed together, to ensure replicability of findings. For imaging experiments, we used at least 5 biological replicates per experimental condition. For histology experiments, we used at least 3 biological replicates per experimental condition. All attempts at replication were successful.
Randomization	Male and female mice were randomly allocated into experimental groups, ensuring that each sex was approximately equally represented in each group. For experiments involving diet-induced obesity, groups were pseudo-randomly generated to ensure that both groups were matched for body weight.
Blinding	Investigators collecting (e.g, performing behavioural measurements) or analyzing (e.g., counting neurons) data were blinded to experimental conditions.

Reporting for specific materials, systems and methods

We require information from authors about some types of materials, experimental systems and methods used in many studies. Here, indicate whether each material, system or method listed is relevant to your study. If you are not sure if a list item applies to your research, read the appropriate section before selecting a response.

Materials & experimental systems

n/a	Involved in the study
☐	☒ Antibodies
☒	☐ Eukaryotic cell lines
☒	☐ Palaeontology and archaeology
☐	☒ Animals and other organisms
☒	☐ Clinical data
☒	☐ Dual use research of concern

Methods

n/a	Involved in the study
☒	☐ ChIP-seq
☒	☐ Flow cytometry
☒	☐ MRI-based neuroimaging

Antibodies

Antibodies used

sheep anti-EGFP (1:1000, 4745-1051, Lot 1710, Bio-Rad)
rabbit anti-RFP (1:1000, 600-401-379, Lot 46510, Rockland)
donkey anti-sheep IgG Alex488 (1:500, 713-545-147, Lot 146368, Jackson ImmunoReseasrch)
donkey anti-rabbit IgG Cy3 (1:500, 711-165-152, Jackson, Lot 145930, ImmunoResearch)

Validation

Primary antibodies were used to amplify virally-expressed fluorophore expression and have been validated in previous publications. Information on validation and citations can be found:

For sheep anti-EGFP (92 citations): https://www.citeab.com/antibodies/111142-4745-1051-sheep-anti-green-fluorescent-protein?des=a92c6b1c71f0385b

For rabbit anti-RFP (1129 citations): https://www.citeab.com/antibodies/1908633-600-401-379-anti-rfp-rabbit-antibody-min-x-hu-ms-a?des=0ec4a501cc3935ee

Animals and other research organisms

Policy information about studies involving animals; ARRIVE guidelines recommended for reporting animal research, and Sex and Gender in Research

Laboratory animals

Adult (>8 weeks old) male and female Glp1r-IRES-Cre (029283, Glp1rtm1.1(cre)Lbrl/RcngJ, Jackson Labs), Ai9 (007909, B6.Cg-Gt(ROSA)26Sortm9(CAG-tdTomato)Hze/J, Jackson Labs), Glp1rtm1Ssis (Glp1rfl/fl, MGI:5637837, a gift from Randy Seeley), and C57BL/6J (000664, Jackson Labs) mice were bred and used for all experiments. Mice were group housed (maximum of 5 mice/cage) on a 12 h light/12 h dark cycle at 22°C with ad libitum access to rodent chow (5001, LabDiet) and water unless otherwise noted in the manuscript. Humidity was maintained on average at 55%.

Wild animals

The study did not involve wild animals.

Reporting on sex

Sex was determined at weaning by ano-genital distance and confirmed again prior to experimentation. Male and female mice were used for experimentation, except for one experiment (Fig. 1e) where only males were used to avoid the confounding variable of time post-neural ablation, because our female mice did not achieve diet-induced obesity with 8 weeks of high-fat diet exposure. Except for one experiment (Extended Data Fig. 1f) which had a smaller but still significant effect in female compared to male mice, we did not observe any significant sex differences in any analyses and therefore we combined results for males and females.

Field-collected samples

The study did not involve samples collected from the field.

Ethics oversight

All procedures were approved by the Monell Chemical Senses Center Institutional Animal Care and Use Committee.

Note that full information on the approval of the study protocol must also be provided in the manuscript.